

1 **Bed and width oscillations form coherent patterns in a partially confined,**
2 **regulated gravel-cobble bedded river adjusting to anthropogenic disturbances**

3

4

5 Rocko A. Brown^{*1,2} and Gregory B. Pasternack¹

6

7 1-University of California, Davis, One Shields Avenue, Davis, CA, USA.

8 2-Environmental Science Associates, 2600 Capitol Avenue, Suite 200, Sacramento, CA

9 USA

10 * Corresponding author. Tel.: +1 510-333-5131; E-mail: rokbrown@ucdavis.edu.

11

12

13

14

15 **Abstract**

16 Understanding the spatial organization of river systems in light of natural and
17 anthropogenic change is extremely important, because it can provide information to
18 assess, manage and restore them to ameliorate worldwide freshwater fauna declines.
19 For gravel and cobble bedded alluvial rivers studies spanning analytical, empirical and
20 numerical domains suggest that at channel-forming flows there is a tendency for
21 covarying bankfull bed and width undulations amongst morphologic units such as pools
22 and riffles whereby relatively wide areas have relatively higher minimum bed elevations
23 and relatively narrow areas have relatively lower minimum bed elevations. The goal of
24 this study was to determine whether minimum bed elevation and flow-dependent
25 channel top width are organized in a partially confined, incising gravel-cobbled bed river
26 with multiple spatial scales of anthropogenic and natural landform heterogeneity across
27 a range of discharges. A key result is that the test river exhibited covarying oscillations
28 of minimum bed elevation and channel top width across all flows analyzed. These
29 covarying oscillations were found to be quasi-periodic at channel forming flows, scaling
30 with the length scales of bars, pools and riffles. Thus it appears that alluvial rivers
31 organize their topography to have quasi-periodic shallow and wide and narrow and
32 deep cross section geometry, even despite ongoing, centennial-scale incision.
33 Presumably these covarying oscillations are linked to hydrogeomorphic mechanisms
34 associated with alluvial river channel maintenance. The biggest conclusion from this
35 study is that alluvial rivers are defined more so by variability in topography and flow,
36 than mean conditions. Broader impacts of this study are that the methods provide a
37 framework for characterizing longitudinal and flow dependent variability in rivers for

38 assessing geomorphic structure and aquatic habitat in space, and if repeated, through
39 time.

40

41 **1. Introduction**

42 Understanding the spatial organization of river systems in light of natural and
43 anthropogenic change is extremely important, because it can provide information to
44 assess, manage and restore them to ameliorate worldwide freshwater fauna declines
45 (Frissell et al., 1986; Richter et al., 1997). Alluvial rivers found in transitional upland-
46 lowland environments with slopes < 0.02 and median diameter bed sediments ranging
47 from 8 to 256 mm can exhibit scale dependent organization of their bed sediments
48 (Milne, 1982), bed elevation profile (Madej, 2001), cross section geometry (Rayberg and
49 Neave, 2008) and morphological units (Keller and Melhorn, 1978; Thomson et al.,
50 2001). For these rivers a plethora of studies spanning analytical, empirical and
51 numerical domains suggest that at channel-forming flows there is a tendency for
52 covarying bankfull bed and width undulations amongst morphologic units such as pools
53 and riffles (Brown et al., 2016). That is, relatively wide areas have higher relative bed
54 elevations and relatively narrow areas have lower relative bed elevations. While
55 covarying bed and width undulations have been evaluated in field studies using cross
56 section data (Richards, 1976a,b), in models of sediment transport and water flow
57 (Repetto and Tubino, 2001), flume studies (Nelson et al., 2015) and in theoretical
58 treatments (Huang et al., 2004), this idea has never been evaluated in a
59 morphologically dynamic river corridor for which a meter-scale digital elevation model is
60 available across a wide range of discharges, from a fraction of to orders of magnitude

61 more than bankfull. The goal of this study was to understand if and how bed elevation
62 and flow-dependent channel width are organized in a partially confined, incising,
63 regulated gravel-cobble bed river with multiple spatial scales of landform heterogeneity
64 across a range of discharges. The analysis of geometric organization was accomplished
65 through a suite of spatial series analyses using a 9km reach of the lower Yuba River
66 (LYR) in California, USA as a testbed. Our central hypothesis is that the test river reach
67 will have covarying and quasi-periodic bed and width oscillations. Due to the test river
68 corridor's variability (White et al., 2010), , past history (James et al., 2009), and having a
69 Mediterranean climate(Wolman and Gerson, 1978) these patterns may be dominant in a
70 range of flows. Knowledge of spatial patterns are commonly used to infer the
71 geomorphic processes that yielded those patterns (Davis, 1909; Thornbury, 1954)
72 and/or what future processes will be driven by the current spatial structure of landforms
73 (Leopold and Maddock, 1953; Schumm, 1971; Brown and Pasternack, 2014). However,
74 such inferences rarely include transparent, objective spatial analysis of topographic
75 structure, so this study demonstrates a new methodology accessible to most
76 practitioners to substantiate the ideas behind the process-morphology linkages they
77 envision to be driven by variability in topography. The results of the study contribute to
78 basic knowledge by showing multiple layers of coherent structure between width and
79 bed undulations, which alerts geomorphologists to the need to prioritize future research
80 on the cause and consequences of structured channel variability as opposed to further
81 work on the central tendency of morphological metrics.

82

83 1.1 *Background*

84 A multitude of numerical, field, and theoretical studies have shown that gravel
85 bed rivers have covarying oscillations between bed elevation and channel width related
86 to riffle-pool maintenance processes. The joint periodicity in oscillating thalweg and
87 bankfull width series for pool-riffle sequences in gravel bed rivers was identified by
88 Richards (1976b) who noted that riffles have widths that are on average greater than
89 those of pools, and he attributed this to flow deflection over riffles into the channel
90 banks. Since then, many studies related to processes that rejuvenate or maintain the
91 relief between bars and pools (i.e., “maintenance” or “self-maintenance”) have implied a
92 specific spatial correlation of width and depth between the pool and riffle at the bankfull
93 or channel forming discharge (e.g. Wilkinson et al. 2004; MacWilliams et al., 2006;
94 Caamano et al., 2009; Thompson, 2010). For example, Caamano et al. (2009) derived a
95 criterion for the occurrence of a mean reversal in velocity (Keller, 1971) that implies a
96 specific correlation of the channel geometry of alluvial channels with undulating bed
97 profiles. Specifically, for a reversal in mean velocity at the bankfull or channel forming
98 discharge (holding substrate composition constant), the riffle must be wider than the
99 pool and the width variation should be greater than the depth variation between the riffle
100 and residual pool depth. Milan et al. (2001) evaluated several riffle-pool couplets, from
101 a base flow to just over the bankfull discharge. They found that convergence and
102 reversals in section-averaged velocity and shear stress were complex and non-uniform,
103 which suggests that different morphologic units may be maintained at different
104 discharges. Wilkinson et al. (2004) explicitly showed that phase shifts in shear stress
105 from the riffle to the pool between high and low discharge required positively covarying

106 bed and width undulations. White et al. (2010) showed how valley width oscillations
107 influence riffle persistence despite larger channel altering floods and interdecadal valley
108 incision. Sawyer et al (2010) used two-dimensional (2D) hydrodynamic modeling and
109 digital elevation model (DEM) differencing to illustrate how variations in wetted width
110 and bed elevation can modulate regions of peak velocity and channel change at a pool-
111 riffle-run sequence across a range of discharges from 0.15 to 7.6 times bankfull
112 discharge. DeAlmeida and Rodriguez (2012) used a 1D morphodynamic model to
113 explore the evolution of riffle-pool bedforms from an initially flat bed, while maintaining
114 the channel width variability. The resulting simulations were in close agreement to the
115 actual bed profile in their model. Thus, their study is another example that channel
116 width can exert controls on the structure of the bed profile. The flows at which the above
117 processes are modulated vary in the literature.

118 From a system perspective, bed and width undulations, both jointly and in
119 isolation, are a means of self-adjustment in alluvial channels that minimize the time rate
120 of potential energy expenditure per unit mass of water in accordance with the law of
121 least time rate of energy expenditure (Langbein and Leopold, 1962; Yang, 1971;
122 Cherkauer, 1973; Wohl et al., 1999). For bed profiles, Yang (1971) and Cherkauer
123 (1973) showed that undulating bed relief is a preferred configuration of alluvial channels
124 that minimize the time rate of potential energy expenditure. Using field, flume, and
125 numerical methods Wohl et al. (1999) showed that valley wall oscillations also act to
126 regulate flow energy analogous to bedforms. In analyzing reach scale energy
127 constraints on river behavior Huang et al. (2004) quantitatively showed that
128 wide/shallow sections and deep/narrow sections are two end member cross sectional

129 configurations necessary for efficiently expending excess energy for rivers, so these two
130 types of cross sections imply covarying bed and width undulations as a means of
131 expending excess energy. Therefore the above studies suggest that both bed and
132 width oscillations are a means to optimize channel geometry for the dissipation of
133 excess flow energy. The question now is the extent to which this well-developed theory
134 plays out in real rivers, especially now that meter-scale river DEMs are available.

135 Flows that drive channel maintenance in Western U.S. rivers, such as the test
136 river in this study (described in detail in Section 3 below), are thought to typically have
137 recurrence intervals ranging from 1.2 to 5 years (Williams, 1978; Andrews, 1980; Nolan
138 et al., 1987). Most of the literature investigating riffle-pool maintenance discussed above
139 report bedform sustaining flow reversals occurring at or near bankfull, often with no
140 specificity to the frequency of these events (Lisle, 1979; Wilkinson et al., 2004). Studies
141 that do report recurrence intervals have ranged from the 1.2 to 7.7 year recurrence
142 flows (Keller, 1971; Sawyer et al., 2010). However, many rivers exhibit multiple scales
143 of freely formed and forced landscape heterogeneity that should influence fluvial
144 geomorphology when the flow interacts with them, no matter the magnitude (Church,
145 2006; Gangodagamage et al., 2007). For example, Strom and Pasternack (2016)
146 showed that the geomorphic setting can influence the stage at which reversals in peak
147 velocity occur. In their study an unconfined anastomizing reach experienced velocity
148 reversals at flows ranging from 1.5 to 2.5 year recurrence flows, compared to 2.5 to 4.7
149 year recurrence flows for a valley-confined reach. Given that river geometry can record
150 memory from past floods (Yu and Wolman, 1987), and the presence of multiple layers
151 of topographic variability (Brown and Pasternack, 2014), it is hypothesized that

152 covarying bed and width undulations could also be present at discharges other than
153 bankfull.

154

155 1.2 Study Objectives

156 The primary objectives of this study were to determine if there are covarying bed
157 and width oscillations in the test reach, if they exhibit any periodicity, and how they vary
158 with discharge. Based on the literature review above, we hypothesize there will be
159 covarying bed and width oscillations that form quasi-periodic patterns, with the strongest
160 relationship occurring for a broad range of channel forming flows. A secondary objective
161 is to demonstrate how a geomorphic covariance structure (GCS) analysis of minimum
162 bed elevation and wetted width, as defined below, can be generated from high-
163 resolution topography and hydraulic models to assess flow-dependent spatial
164 organization of river corridor topography. The study site was a 6.4-km section of the
165 lower Yuba River (LYR), an incising and partially confined self-formed gravel-cobble
166 bedded river (Figure 1; described in Section 3). Several statistical tests were used on
167 the serial correlation of minimum bed elevation, Z , channel top width, W^j , and their
168 geomorphic covariance structure, $C(Z, W^j)$, where j indexes the flow discharge. The
169 novelty of this study is that it provides the first assessment of covarying bed and width
170 oscillations in a partially confined, self-maintained alluvial river across a wide array of
171 flows. The broader impact is that it provides a framework for analyzing the flow
172 dependent topographic variability of river corridors, without differentiating between
173 discrete landforms such as riffles and pools. Further, an understanding of the flow
174 dependent spatial structure of bed and width GCS would be useful in assessing their

175 utility in applied river corridor analysis and synthesis for river engineering, management
176 and restoration.

177

178 **2. Experimental Design**

179 To evaluate covarying bed and width undulations, the concepts and methods of
180 geomorphic covariance structures were used (Brown, 2014; Brown and Pasternack,
181 2014). A GCS is a bivariate spatial relationship amongst or between variables along a
182 pathway in a river corridor. It is not a single metric as in statistical covariance, but a
183 spatial series, and hence can capture spatially explicit geomorphic structure. Variables
184 assessed can be flow-independent measures of topography (e.g., bed elevation,
185 centerline curvature, and cross section asymmetry) and sediment size as well as flow-
186 dependent hydraulics (e.g., top width, depth, velocity, and shear stress; Brown, 2014),
187 topographic change, and biotic variables (e.g., biomass and habitat utilization).

188 Calculation of a GCS from paired spatial series is straightforward by the product
189 $x_{std,i} * y_{std,i}$, where the subscript *std* refers to standardized and possibly detrended
190 values of two variables *x* and *y* at location *i* along the centerline, creating the serial data
191 set $C(X, Y)$. Since this study is concerned with bed and flow dependent top width
192 undulations, the GCS at each flow *j* is denoted as $C(Z, W^j)$. More information on GCS
193 theory is provided in section 4.2 below. GCS series were generated for eight flows
194 ranging from 8.50 to 3,126 m³/s, spanning a broad range of flow frequency (Table 1).
195 The range of selected flows spans a low flow condition up to the flow of the last large
196 flood in the river.-These flows were selected to provide enough resolution to glean flow-
197 dependent effects, while not producing redundant results.

198 The first question this study sought to answer was whether there was a tendency for
199 covarying Z and W^j and how it changed with discharge. If Z and W^j covary then the
200 sign of the residuals of both variables will both be positive or negative yielding a
201 positive $C(Z, W^j) > 0$. Therefore, to determine if there are covarying bed and width
202 oscillations a histogram was generated for each flow dependent series of $C(Z, W^j)$. The
203 second question was whether each flow dependent series of $C(Z, W^j)$ was random,
204 constant, periodic or quasi-periodic. Quasi-periodicity in this setting is defined as a
205 series with periodic and random components, as opposed to purely random or purely
206 periodic (Richards, 1976a). Quasi-periodicity differs from periodic series in that there
207 are elements of randomness blended in (Newland, 1993). To answer this question
208 autocorrelation function (ACF) and power spectral density (PSD) analyses of each
209 $C(Z, W^j)$ series were used to determine if there were statistically significant quasi-
210 periodic length scales (sensu Carling and Orr, 2002) at which $C(Z, W^j)$ covary and how
211 that changes with discharge.

212 Based on the studies listed above (Section 1.1), we hypothesize that gravel-cobble
213 bedded rivers capable of rejuvenating their riffle-pool relief should exhibit a topography
214 (at any instant in time) with a tendency for quasi-periodic and covarying bed and width
215 oscillations. The basis for covarying and quasi-periodic bed and width oscillations is
216 founded on the idea that, on average, channel geometry is maintained during bankfull
217 (e.g. geometric bankfull) discharge and that locally channels are shaped by riffle-pool
218 maintenance mechanisms (Wilkinson et al. 2004; MacWilliams et al., 2006; Caamano et
219 al., 2009; Thompson, 2010). Based on the literature reviewed in Section 1.1 we
220 hypothesize that the $C(Z, W^j)$ GCS will, on average, become more positive with

221 increasing flow until approximately the bankfull discharge, where the channel overtops
222 its banks and non-alluvial floodplain features exert control on cross-sectional mean
223 hydraulics. At that point there may not be a tendency for positive or negative residuals,
224 if the topographic controls at that flood stage are not important enough to control
225 channel morphology. For example, smaller events might occur frequently enough to
226 erase the in-channel effects of the large infrequent events, especially in a temperate
227 climate (Wolman and Gerson, 1978). On the other hand, if a system is dominated by the
228 legacy of a massive historical flood and lacks the capability to recover under more
229 frequent floods, then the $C(Z, W^j)$ GCS will continue to increase until the discharge that
230 carved out the existent covarying bed and width oscillations for the current topography
231 is revealed. Note that we do not expect a clear threshold where organization in the
232 $C(Z, W^j)$ GCS is a maximum, but rather a range of flows near the bankfull discharge.
233 The effect of a particular flow on a channel is dependent not just on that flow, but the
234 history of flow conditions that led to the channel's condition (Yu and Wolman, 1987).
235 Therefore, it should not be expected that the observed patterns will be associated with a
236 singular flow value. Also, this study looked at a river in a Mediterranean climate, and
237 thus it may be more prone to exhibiting a wider range of positive $C(Z, W^j)$ GCS than a
238 temperate or tropical river, as the number and frequency of recovery processes is
239 reduced (Wolman and Gerson, 1978). With this logic, it is hypothesized that the
240 $C(Z, W^j)$ GCS will be quasi-periodic for flows near the bankfull discharge, due to the
241 presence of bar and pool topography, and that the ACF and PSD will yield length scales
242 commensurate with the average spacing of these topographic features. For flows
243 above the bankfull discharge, a river corridor has many local alluvial landforms, bedrock

244 outcrops and artificial structures on its floodplain and terraces. These features influence
245 bed adjustment during floods that engage them, and hence impact the GCS. It is
246 unknown how GCS length scales will change in response to the topographic steering
247 these features induce causing changes to bed elevation, but investigating that is a novel
248 and important aspect of this study. In addition to performing these tests we also present
249 two ~ 1.4-km sections of the $C(Z, W^j)$ GCS, Z , W and the detrended topography for
250 three representative flows to discuss specific examples of how these patterns change
251 with landforms in the river corridor across a wide array of discharges.

252 Limitations to this study (but not the GCS approach) for worldwide generalization
253 include not considering other variables relevant to how alluvial rivers adjust their shape,
254 such as grain size, channel curvature and vegetation, to name a few. Some of these
255 limitations were not study oversights, but reflected the reality that the study reach used
256 had relatively homogenous sediments (Jackson et al., 2013), low sinuosity, and limited
257 vegetation (Abu-Aly et al., 2014). This yielded an ideal setting to determine how much
258 order was present for just bed elevation and channel width, but does not disregard the
259 importance of these other controls, which can be addressed in future studies at suitable
260 sites. Also, this study is not a direct test of the response to or drivers of morphodynamic
261 change. The extent to which GCS can be used as an indicator of change to greatly
262 simply geomorphic analysis instead of doing morphodynamic modeling remains
263 unknown, but finding metrics that link landforms, the agent that shape them, and the
264 responses they induce has always been the goal of geomorphology (Davis, 1909).

265

266 3. Study Area

267 3.1 *River context*

268 The study area was the 6.4-km Timbuctoo Bend Reach of the lower Yuba River
269 (LYR) in northeastern California, USA. The reach begins at the outlet of a bedrock
270 canyon that is dammed ~ 3-km upstream, and the watershed above the dam drains
271 3480 km² of dry summer subtropical mountains. Little is known about the pre-European
272 Yuba River, but in this reach it is confined by valley hillsides and bedrock outcrops, and
273 these are evident in some photos from early European settlers panning the river for gold
274 in the late 1840s. During the mid to late 19th century there was a period of extensive
275 hydraulic gold mining of hillside alluvial deposits in the upper Yuba watershed that
276 delivered an overwhelming load of heterogeneous sediment to the lowland river valley
277 (James et al., 2009). Geomorphologist G. K. Gilbert photo documented the LYR around
278 the time of its worst condition in the early 20th century and provided foundational
279 thinking related to how the river would evolve in time (Gilbert, 1917). In 1941
280 Englebright Dam was built to hold back further sediment export from the mountains, and
281 that allowed the river valley to begin a process of natural recovery, which was reviewed
282 by Adler (1980) and more recently by Ghoshal et al. (2010). However, this process was
283 interfered with by widespread dredger mining in the early to mid 20th century. In two
284 locations of the study reach there are wide relict dredger tailings piles on the inside of
285 the two uppermost meander bends that the river has been gradually eroding.

286 The hydrology of the regulated LYR is complex and quite different from the usual
287 story of significantly curtailed flows below a large dam. Englebright Dam primarily
288 serves as a sediment barrier and it is kept nearly full. As a result, it is operated to

289 overtop when outflow is $> 127.4 \text{ m}^3/\text{s}$ long enough to fill its small remaining capacity, so
290 flood hydrology is still seasonal and driven by rainfall and snowmelt in the watershed.
291 Two of three sub catchments do not have large dams, so winter floods and spring
292 snowmelt commonly cause spill over Englebright sufficient to exceed the bankfull
293 channel in Timbuctoo Bend. The one regulated sub catchment does have a large dam,
294 New Bullards Bar (closed in 1970), and this reduces the frequency and duration of
295 floodplain inundation compared to the pre-dam record (Escobar-Arias and Pasternack,
296 2011; Cienicala and Pasternack, in press), but not like other rivers where the entire
297 upstream watershed is regulated. Sawyer et al. (2010) reported the 1.5 year recurrence
298 interval for the post Englebright, pre New Bullards Bar period as $328.5 \text{ m}^3/\text{s}$ and then for
299 post New Bullards Bar as $159.2 \text{ m}^3/\text{s}$. California has long been known to exhibit a
300 roughly decadal return period for societally important major floods that change river
301 courses (Guinn, 1890), though the magnitude of those floods is not necessarily a 10-
302 year recurrence interval scientifically. Since major flow regulation in 1970, the three
303 largest peak annual daily floods came roughly 10 years apart, in the 1986, 1997, and
304 2006 water years. The flood of 1997 was the largest of the post-dam record. The 2006
305 peak flood event had a recorded peak 15-minute discharge of $3126.2 \text{ m}^3/\text{s}$ entering the
306 study reach.

307 Wyrick and Pasternack (2012) analyzed LYR inundation patterns in a high-
308 resolution DEM of the river produced after the 2006 wet season, and they considered
309 how channel and floodplain shapes change dramatically through the study reach. Their
310 findings apply to the Timbuctoo Bend Reach. Different locations exhibited spillage out of
311 the channel into low-lying peripheral swales and onto lateral and point bars at flows

312 from ~ 84.95-141.6 m³/s. When the water stage rises to 141.6 m³/s, relatively flat active
313 bar tops become inundated and the wetted extents line up with the base of willows
314 along steeper banks flanking the channel. These and other field indicators led to the
315 consideration of 141.6 m³/s as representative of the bankfull discharge adjusted to the
316 modern regulated flow regime since 1970. By a flow of 198.2 m³/s, banks are all
317 submerged and water is spilling out to various degrees onto the floodplain. The
318 floodplain is considered fully inundated when the discharge reaches 597.5 m³/s. Above
319 that flow stage exist some terraces, bedrock outcrops, and soil-mantled hillsides that
320 become inundated. For the two relict dredger tailings piles mentioned earlier, they
321 interact with the flows ranging from 597.5-1,195 m³/s. Apart from these piles, the flow
322 width interacts predominately with the valley walls for discharges at 1,195 m³/s and
323 above. Given the estimate of bankfull discharge for the LYR, the instantaneous peak
324 flow during the 2006 flood was ~ 23 times that, so quite substantial compared to those
325 commonly investigated in modern geomorphic studies.

326

327 3.2 *Timbuctoo Bend details*

328 A lot is known about the geomorphology of Timbuctoo Bend, and this information
329 helps inform this study to substantiate the possibility that the river's topography is
330 organized in response to differential topographic steering as a function of flow stage.
331 According to Wyrick and Pasternack (2012), the reach has a mean bed slope of 0.002,
332 a thalweg length of 6337 m, a mean bankfull width of 84 m, a mean floodway width of
333 134 m, an entrenchment ratio of 2.1 (defined per Rosgen, 1996), and a weighted mean
334 substrate size of 164 mm. Using the system of Rosgen (1996), it classifies as a B3c

335 stream, indicating moderate entrenchment and bed slope with cobble channel material.
336 A study of morphological units revealed that its base flow channel area consists of 20%
337 pool, 18% riffle, and then a mix of six other landform types. More than half of the area of
338 the riverbank ecotone inundated between base flow and bankfull flow is composed of
339 lateral bars, with the remaining area containing roughly similar areas of point bars,
340 medial bars, and swales (Wyrick and Pasternack, 2012). A study of bankfull channel
341 substrates found that they are differentiated by morphological unit type, but the median
342 size of all units is in the cobble range (Jackson et al., 2013), even depositional bars that
343 are often thought of as relatively fine in other contexts. Vegetated cover of the river
344 corridor ranged from 0.8 to 8.1% of the total wetted area at each flow, with more
345 inundated vegetation at higher flows.

346 White et al. (2010) used a sequence of historical aerial photos, wetted channel
347 polygons, repeat long profiles from 1999 and 2006, and a valley width series to
348 conclude that even though Timbuctoo Bend has incised significantly since 1942 in
349 response to many floods, there are several riffles and pools that persist in the same
350 wide and constricted valley locations, suggesting that valley width oscillations maintain
351 those positions and drive morphodynamic response. This suggests that it may not
352 matter exactly which instant topography one might analyze to look at the effect of
353 topographic variability in controlling or responding to large flood processes, as they all
354 should reflect the same topographic steering regime induced by the valley walls.

355 Two studies have been done to look at the hydraulic processes associated with
356 different flood stages in Timbuctoo Bend. Sawyer et al. (2010) found that one of the
357 pool-riffle-run units in this reach experienced flow convergence routing between

358 baseflow, bankfull flow, and a flow of roughly eight times bankfull discharge that
359 maintained riffle relief. Strom et al. (2016) assessed the hydraulics of the whole reach
360 over the same range of flows in this study, and they reported that the reach exhibits a
361 diversity of stage-dependent shifts in the locations and sizes of patches of peak velocity.
362 The spatial persistence of such patches decreased with discharge until flows exceeded
363 $\sim 1000 \text{ m}^3/\text{s}$, at which point valley walls sustained their location for flows up to the peak
364 of $3,126 \text{ m}^3/\text{s}$. Also, peak-velocity patches resided preferentially over chute and riffle
365 landforms at within-bank flows, several morphological unit types landforms for small
366 floods, and pools for floods $> 1000 \text{ m}^3/\text{s}$. These studies corroborate the process
367 inferences made by White et al. (2010) in that hydraulics were found to be stage-
368 dependent in ways that were consistent with the mechanism of flow convergence
369 routing.

370 Finally, Carley et al. (2012), Wyrick and Pasternack (2015), and Pasternack and
371 Wyrick (in press) used DEM differencing, uncertainty analysis, scale-stratified sediment
372 budgeting, and topographic change classification to analyze how the LYR changed from
373 1999-2008, including Timbuctoo Bend. These studies took advantage of the repeated
374 mapping of the LYR in 1999 and 2006-2008, with Timbuctoo Bend mapped entirely in
375 2006. They found large amounts of erosion and deposition, strong differential rates of
376 change among different landforms at three spatial scales, and topographic changes
377 driven by 19 different geomorphic processes. For Timbuctoo Bend, the dominant
378 topographic change processes found were in-channel downcutting (including knickpoint
379 migration) and overbank (i.e., floodplain) scour, with noncohesive bank migration a
380 distant third. Thus, the river appears to change through adjustments to its bed elevation

381 far more than changes to its width in this reach. This finding will come into play in
382 interpreting the results of this study later on.

383 In summary, even with modern technology it is impossible to monitor the
384 hydrogeomorphic mechanics of fluvial change in a large river for flows up to 22 times
385 bankfull discharge, so recent studies have tried to get at the mechanisms during such
386 events with a range of strategies. Historical river analysis, hydrodynamic modeling, and
387 topographic change detection and analysis have been used together to reveal a picture
388 of a river that is changing in response to multiple scales of landform heterogeneity that
389 drive topographic steering. Even though the river has changed through time, there has
390 been a persistence of nested landforms, and thus it would be useful to understand how
391 topographic features are organized purely through an analysis of the DEM per the
392 methods developed in this study. This study exclusively uses the 2006 map made
393 during the dry season that followed the dramatic 2006 wet season, which included the
394 large flood, two other notable peaks, and a total of 18 days of floodplain filling flow.
395 Thus it addresses the topography as it existed after that river-altering wet season and
396 how it will in turn influence the dynamics of the next one.

397

398 **4. Methods**

399 The meter-scale topographic map of Timbuctoo Bend produced from
400 echosounder and robotic total station ground surveys were used for extraction of Z
401 (Carley et al., 2012; see Supplemental Materials), while a corresponding meter-scale
402 2D hydrodynamic model was used to generate data sets for W^j for each discharge.
403 Details about the 2D model are documented in the Supplemental Materials and

404 previous publications (Abu-Aly et al., 2013; Wyrick and Pasternack, 2014; Pasternack et
405 al., 2014); it was thoroughly validated for velocity vector and water surface elevation
406 metrics, yielding outcomes on par or better than other publications using 2D models.

407 *4.1 Data Extraction*

408 A first step was to extract Z and W^j spatial series from the digital elevation model
409 and 2D model outputs. This required having a sample pathway along which bed
410 elevation could be extracted from the DEM and top width from the wetted extents from
411 the 2D model. Sampling river widths was done using cross sections generated at even
412 intervals perpendicular to the sample pathway and then clipped to the 2D model derived
413 wetted extent for each flow. Because of this, the pathway selected can have a
414 significant bearing on whether or not sample sections represent downstream oriented
415 flow or overlap where pathway curvature is high. There are several options in
416 developing an appropriate pathway for sampling the river corridor. The thalweg is
417 commonly used in flow-independent geomorphic studies, but the thalweg is too tortuous
418 within the channel to adhere to a reasonable definition of top width. Further, as flow
419 increases, central flow pathway deviates from the deepest part of the channel due to
420 higher flow momentum and topographic steering from submerged and partially
421 submerged topography (Abu-Aly et al., 2014). Therefore, in this study we manually
422 developed flow-dependent sample pathways using 2D model hydraulic outputs of depth,
423 velocity and wetted area. The effect of having different sample pathways for each flow is
424 that it accounts for flow steering by topographic features in the river corridor.

425 For each flow a grid of kinetic flow energy ($d_i * v_i^2$) was generated in ARCGIS®,
426 where d_i is the depth and v_i is the velocity at node i in the 2D model hydraulics rasters.

427 Then a sample pathway was manually digitized using the momentum grid, following the
428 path of greatest kinetic energy. For flow splits around islands, if the magnitude of
429 energy in one channel was more than twice as great as the other it was chosen as the
430 main pathway. If they were approximately equal then the pathway was centered
431 between the split. Once a sample pathway was developed it was then smoothed using
432 a Bezier curve approach over a range of 100 m, or approximately a bankfull channel
433 width to help further minimize section overlaps. For each sample pathway cross
434 sections were generated at 5 m intervals and clipped to the wetted extent of each flow,
435 with any partially disconnected backwater or non downstream oriented areas manually
436 removed.

437 Despite smoothing there were areas of the river where the river has relatively
438 high curvature in the sample pathway causing sample section overlaps to occur. These
439 were manually edited by visually comparing the sample sections with the kinetic flow
440 energy grid and removing overlapped sections that did not follow the downstream flow
441 of water. This was more prevalent at the lower discharges than the higher ones due to
442 the effects topographic steering creating more variable sample pathways.

443 To provide a constant frame of spatial reference for comparison of results
444 between flows, while preserving flow-dependent widths, sections were mapped to the
445 lowest flow's sample pathway using the spatial join function in ARCGIS®. The lowest
446 flow was used, because that had the longest path. This insures no multiple-to-one
447 averaging of data would happen, as that would otherwise occur if data were mapped
448 from longer paths to shorter ones. To create evenly spaced spatial series the data was
449 linearly interpolated to match the original sampling frequency of 5 m. For Z the minimum

450 bed elevation along each section was sampled from the DEM using the same sections
451 for measuring width for the lowest flow sample pathway.

452

453 4.2 *Developing geomorphic covariance structures*

454 To generate GCS series for bed and flow-dependent width undulations the two
455 variables, Z and W^j were first detrended and standardized. Detrending is not always
456 needed for width in GCS analysis, but some analyses in this study did require it. A linear
457 model was used for Z , (Table 2) as is common in many studies that analyze reach scale
458 bed variations (Melton, 1962, Richards, 1976a; McKean et al., 2008). Similarly, each
459 W^j series was linearly detrended, but the trends were extremely small, with a consistent
460 slope of just 0.002 (Table 2). Finally, each series was standardized by the mean and
461 variance of the entire detrended series (Salas et al., 1980) to achieve second order
462 stationarity, which is a prerequisite for spectral analysis (described in the following
463 section). Second order stationarity of a series means that the mean and variance across
464 the domain of analysis are constant (Newland, 1983). Removal of the lowest frequency
465 of a signal, which can often be visually assessed, has little impact upon subsequent
466 spectral analyses (Richards, 1979). A linear trend was used over other options such as
467 a polynomial, because a linear trend preserves the most amount of information in the
468 bed series, while a polynomial can filter out potential oscillations. After detrended and
469 standardized series of Z and W^j were generated, then the GCS between them was
470 computed by taking the product of the two at each centerline station, yielding a spatially
471 explicit measure of how the two covary (Figure 2). The GCS is the whole series of
472 $C(Z, W^j)$ values and not a single metric such as the traditional statistical definition of

473 covariance. Interpretation of a GCS is based on the sign, which in turn is driven by the
474 signs of contributing terms. For $C(Z, W^j)$, if both Z and W^j are positive or negative then
475 $C(Z, W^j) > 0$, but if only one is negative then $C(Z, W^j) < 0$. For $C(Z, W^j)$ these
476 considerations yield four sub-reach scale landform end members that deviate from
477 normative conditions (Figure 3). Normal conditions in this context refer to areas where
478 both variables are close to the mean and thus $C(Z, W^j) \sim 0$. Note that the signs of Z and
479 W^j are not only important, but the magnitude is, too. Since $C(Z, W^j)$ is generated by
480 multiplication, if either Z or W^j is within the range of -1 to 1, then it serves to discount
481 the other. If Z or W^j is > 1 or < -1 it amplifies $C(Z, W^j)$. We did not assess the statistical
482 significance of coherent landform patterns, but one could do so following Brown and
483 Pasternack (2014).

484

485 4.3 Data Analysis

486 Before any statistical tests were performed we first visually assessed the data in
487 two approximately 1.4-km long sections to illustrate how $C(Z, W^j)$ is affected by flow
488 responses to landforms. For these two examples only three discharges were selected to
489 illustrate flow dependent changes in Z , W^j , and $C(Z, W^j)$ with fluvial landforms. The
490 lowest and highest flows, i.e. 8.50 and 3,126 m³/s, were selected to bracket the range of
491 flows investigated. The intermediate flow selected was 283.2 m³/s based on the shifts in
492 $C(Z, W^j)$ observed in the histogram, ACF and PSD tests as shown below in the results.
493 For these examples the exact magnitudes of $C(Z, W^j)$ are not as important as the
494 patterns and how they relate to visually discernible landforms.

495 A Mann-Whitney U-test was performed between each $C(Z, W^j)$ dataset to

496 determine if they were statistically different at the 95% level. Histograms were then
497 computed for each $C(Z, W^j)$ dataset to evaluate whether there was a tendency for the
498 data to be positively covarying and how that changes with discharge. Two histograms
499 were developed, one based on the quadrant classification of $C(Z, W^j)$ for each flow and
500 another showing the $C(Z, W^j)$ magnitude. This was done so that the distribution of both
501 the type of $C(Z, W^j)$ and magnitudes could be assessed. Additionally, the bivariate
502 Pearson's correlation coefficients (r) were computed between Z and W^j to assess their
503 potential interdependence. Bivariate Pearson's correlation coefficients were also
504 computed each series of W^j . Statistical significance was assessed for (r) using a white
505 noise null hypothesis at the 95% level.

506 Next, ACF and PSD analyses were used to determine if $C(Z, W^j)$ was quasi-
507 periodic or random, as it was visually evident that it was not constant or strictly periodic.
508 If a series is quasi-periodic this will be reflected in statistically significant periodicity in
509 the ACF (Newland, 1993; Carling and Orr, 2000). Because the PSD is derived from the
510 ACF the two tests show the same information, but in different domains, with the ACF in
511 the space domain and the PSD in the frequency domain. So while the ACF analysis
512 reveals periodicity in the signal (if present), the PSD analysis presents the associated
513 frequencies. Both are shown to visually reinforce the results of the PSD analysis. This is
514 helpful because spectral analysis can be very sensitive to the algorithm used and
515 associated parameters such as window type and size. Showing the ACF allows a visual
516 check of dominant length scales that may have quasi-periodicity (e.g. as in Carling and
517 Orr, 2000). The ACF analysis was performed for each flow dependent series of
518 $C(Z, W^j)$ and then these were compared among flows to characterize stage dependent

519 variability and to analyze how spatial structure changed with discharge. This test
520 essentially determines the distances over which $C(Z, W^j)$ are similar. An unbiased
521 estimate of autocorrelation for lags was used:

$$522 \quad R_k = \frac{n}{n-k} \frac{\sum_{i=1}^{n-k} (x_i - \bar{x})(x_{i+k} - \bar{x})}{\sum_{i=1}^{n-k} (x_i - \bar{x})^2} \quad (1)$$

523 where x_i is a value of a GCS series at location i , \bar{x} is the mean value of the GCS (zero
524 due to standardization process) and the terms $\frac{1}{n-k}$ and $\frac{1}{n}$ account for sample bias (Cox,
525 1983; Shumway and Stoffer, 2006). Each R_k versus lag series was plotted against
526 discharge for a maximum of 640 lags (3.2 km, or approximately half the study length),
527 creating a surface that shows how ACF evolves with flow. Lag intervals are equal to
528 sample interval for the datasets (e.g. 5 m). Statistical significance was assessed relative
529 to both white and red noise autocorrelations. White noise is associated with random
530 processes that are uncorrelated in space, while red noise is associated with data that
531 has properties of 1st order autocorrelation (Newland, 1993). The benefit of this approach
532 is that (i) many fluvial geomorphic spatial series display autoregressive properties
533 (Melton, 1962; Rendell and Alexander, 1979; Knighton, 1983; Madej, 2001) and (ii) it
534 provides further context for interpreting results beyond assuming white noise properties.
535 The 95% confidence limits for white noise are given by $-\frac{1}{n} + / - \frac{2}{\sqrt{n}}$ (Salas et al., 1980).
536 For red noise, a first order autoregressive (AR1) model was fit to the standardized
537 residuals for each spatial series of bed elevation and channel width. For comparison,
538 first order autoregressive (AR1) models were produced for 100 random spatial series
539 (each with the same number of points as the flow width spatial series) and averaged.
540 Each averaged AR1 flow width series was then multiplied against the AR1 bed elevation

541 series to create an AR1 model for each $C(Z, W^j)$. The red noise estimate was then
542 taken as the average of all AR1 models of $C(Z, W^j)$. The ACF plots were made so that
543 values not exceeding the white noise significance are not shown, along with a reference
544 contour for the AR1 estimate. Frequencies can be gleaned from the ACF analysis by
545 taking the inverse of the lag distance associated repeating peaks following Carling and
546 Orr (2002).

547 Power spectral density was estimated for each $C(Z, W^j)$ series using a modified
548 periodogram method (Carter et al., 1973). The periodogram is the Fourier transform of
549 the biased estimate of the autocorrelation sequence. The periodogram is defined as:

$$550 \quad P(f) = \frac{\Delta x}{N} \left| \sum_{n=0}^{N-1} h_n x_n e^{-i2\pi f n} \right|^2 \quad (2)$$

551 where $P(f)$ is the power spectral density of x , h_n is the window, Δx is the sample rate,
552 and N is the number of data data points (Trauth et al., 2006). While the raw
553 periodogram can exhibit spectral leakage, a window can reduce this effect. A hamming
554 window was used with a length equal to each data set. Since samples were taken every
555 5 m, this resulted in a sampling frequency of 0.2 cycles/m, and a Nyquist frequency, or
556 cutoff of 0.1 cycles/m. The number of data points used for the analysis was roughly half
557 the largest data set, resulting in a bandwidth of 0.00016 cycles/m. For PSD estimates a
558 modified Lomb-Scargle confidence limit for white noise at the 95% level was used as
559 recommended by Hernandez (1996). Since this study was concerned with changes in
560 PSD with flow, estimates were plotted relative to the standard deviation of all PSD
561 results for all series. This was done instead of using the standard deviation of each
562 series, because that inflates power within a series without context for the variance of
563 adjacent flows.

564

565 **5. Results**

566 *5.1 Relating $C(Z, W^j)$ patterns to landforms*

567 The first example is located at the lower end of the study area and transitions from a
568 valley meander to a straighter valley section with several valley corridor oscillations
569 (Figure 4). Starting upstream there is a large point bar on river left with a pool (i.e., $-Z$)
570 that transitions to a broad riffle with a 200 m long zone with $Z > 1$. Downstream the river
571 channel impinges on the valley walls creating two forced pools with localized negative
572 spikes in Z (Figure 4A,B). Downstream of this the low flow channel is steered to the left
573 of the valley, being bounded by two bars. In this zone Z values are positive and ~ 1 .
574 Past this there is an inset anabranch that transitions to a constricted pool with a broad
575 terrace on river left. In this lower zone Z fluctuates between 0 and -1.

576 Given that bed elevation is held fixed for this type of analysis, changes in W^j act to
577 modulate the sign and magnitude of the $C(Z, W^j)$ GCS with increasing flow. In
578 particular, when Z is near a value of 1, the relative flow W modulates the sign and
579 strength of the GCS signal, with several possible changes including persistence,
580 shifting, reversal, and emergence. For example, a persistent positive W oscillation
581 occurs near station 1500, where this zone is always relatively wide regardless of flow.
582 The anabranch zone however, shows the positive peak in W^j shift downstream from
583 station 900 to 600 from 8.5 to 283.2 m³/s. Two reversals in W^j occur from low to high
584 flow near stations 350 and 1100, which also create reversals in the GCS, but with
585 different signs. Near station 400 Z and W^j are negative at 8.5 and 283.2 m³/s creating
586 a positive GCS. However, W^j increases with flow discharge with an emergent positive

587 peak in W at 3,126 m³/s, that yields a negative GCS.

588 The other example area occurs at a transition from a valley bend to a straighter
589 section where the river transitions from a broad point bar on river left and eventually
590 crosses over between two smaller inset point bars (Figure 5A,B). Starting at the
591 upstream extent a large point bar is located on river left with two forced pools in the
592 channel at approximately 3500 and 3600 that have the strongest negative spikes in Z
593 (Figure 5C,D). Downstream where the point bar ends the bed profile increases with a
594 over a broad riffle with $Z > 1$ located above station 3000. As mentioned above in
595 Section 3, this pool-riffle-run sequence was studied in great detail by Sawyer et al.
596 (2010), who confirmed the occurrence of naturally rejuvenating riffle-pool topography.
597 Immediately below the broad riffle is a localized zone where $Z < 1$ adjacent to a small
598 bedrock outcrop. Within the alternate bars the bed profile is between 0 and 1 for ~ 300
599 m, followed by a localized negative peak in Z around station 2300.

600 For the first 200 m W^j is < 0 for all three flows, but gradually increases downstream
601 with increasing flow (Figure 5C). Since the two deep pools in this initial zone have
602 $Z < 1$, the GCS is > 1 for all flows but reaches a maximum magnitude of 6 at 283.2 m³/s.
603 Beyond this area W^j increases for all flows, but the relative peak broadens and shifts
604 downstream with increasing discharge. At 8.5 m³/s the peak is centered near station ~
605 3000 where it appears a backwater increases flow widths upstream of station 2900. For
606 283.2 m³/s the peak shifts downstream ~ 150 m as the anabranch becomes activated
607 and begins to spread water out. At 3126 m³/s the peak is shifted another ~ 300 m
608 downstream as the bounding point bars are inundated. These shifts in relative W^j act
609 with the bed profile to create a sharper positive peak in $C(Z, W^j)$ near the riffle at low

610 flows, but then this peak dampens and shifts downstream with increasing flow. This is a
611 similar phase shifting reported for a mixed alluvial-bedrock riffle-pool unit reported by
612 Brown and Pasternack (2014), associated with a corresponding phasing of peak
613 velocity from the riffle to the pool with increased flow. Given that the lower ~ 500 m of
614 this example area have $Z \sim 0$ the $C(Z, W^j)$, GCS is also ~ 0 .

615 Overall both examples show that zones where Z was either > 1 or < -1 were
616 associated with large pools and riffles in the study area, and were characterized by
617 strong peaks (e.g. >1) in $C(Z, W^j)$. Patterns of W^j can work with Z to create a variety of
618 flow dependent response including emergence, reversals, amplification and shifting. An
619 interesting result is that most of the locations where $Z < 1$ were short in length, whereas
620 areas where $Z > 1$ tended to be broader in length.

621

622 *5.2 Is there a tendency for positively covarying bed and width oscillations?*

623 The histogram of $C(Z, W^j)$ showed that regardless of discharge, there was a
624 tendency for positive values (e.g. where both Z and W^j covary), and that this changed
625 with stage (Figure 6A). At least 55% of the data always had $C(Z, W^j) > 0$, increasing to
626 68% at 283.2 m³/s, and then slightly declining beyond this flow and stabilizing around
627 60% (Figure 6). There were at most 5% of values < -1 , with an average and standard
628 deviation of 3% and 2%, respectively. Contrasting this, values > 1 peaked at 35% at
629 141.6 m³/s and declined with increasing discharge. So out of the two extremes, the data
630 exhibited a tendency for positive values, with negative values < -1 being very rare.

631 The Mann Whitney U-test showed interesting flow dependent aspects of the
632 $C(Z, W^j)$ data sets, where some ranges of flows were significantly different from each

633 other, and others being similar (Table 3). For example, the 8.50 m³/s $C(Z, W^j)$ had p
634 values that were all significant at the 95% level for each other flow, indicating
635 differences in their distributions. For flows between 28.32-597.5 m³/s, the p values
636 indicated that the series were statistically similar, but not for higher flows. The p values
637 for 1,195, 2,390, and 3,126 m³/s were statistically similar at the 95% level, but not for
638 lower flows.

639 The quadrant-based histogram reveals further insight into the distribution of river
640 geometry with flow (Figure 6B). The average percentage of $C(Z, W^j)$ for each quadrant
641 across all flows was 30% $\{+W, +Z\}$, 14% $\{+W, -Z\}$, 25% $\{-W, +Z\}$, and 31%
642 $\{-W, -Z\}$, with standard deviations ranging from 2-3%. Percentages of positive
643 $C(Z, W^j)$ were relatively evenly distributed between $\{+W, +Z\}$ and $\{-W, -Z\}$, although
644 the latter was slightly more prevalent. The percent of the data in the $\{+W, +Z\}$ quadrant
645 increased from 26% at 8.50 m³/s, peaked at 34% at 597.5 m³/s, decreased to 30% at
646 1195 m³/s and stabilized near this value for higher flows. Meanwhile, the percent of the
647 data in the $\{-W, -Z\}$ quadrant increased from 29% at 8.50 m³/s and peaked at 35% at
648 141.6 - 283.2 m³/s flow, and then decreased to 30% at 597.5 m³/s. After that it
649 increased to 33% and stabilized at and beyond 1,195 m³/s. Both the $\{+W, -Z\}$ and
650 $\{+W, -Z\}$ quadrants followed a similar but opposite trend, reaching a minimum at 283.2
651 m³/s.

652 Further insights into the positive nature of $C(Z, W^j)$ can be inferred from bivariate
653 Pearson's correlation coefficients of Z and W^j (Figure 7). Similar to $C(Z, W^j)$ the flow
654 dependent response was that the correlation between Z and W^j increased with flow
655 until 283.2 m³/s and then subsequently declined. To further reinforce these results one

656 can also inspect the plot of Z, W^j and $C(Z, W^j)$ for $283.2 \text{ m}^3/\text{s}$, visually showing the
657 synchronous nature of Z and W^j (Figure 2) The correlations between combinations of
658 W^j show that each series is significantly correlated to the next highest flow, but there is
659 an interesting flow dependent pattern (Figure 8). Correlations between series decrease
660 with increasing flow, reaching a minimum between 597.5 and $1195 \text{ m}^3/\text{s}$, and then
661 increasing again.

662

663 5.3 *Are bed and width oscillations quasi-periodic?*

664 The ACF of $C(Z, W^j)$ also showed similar changes with discharge as the above
665 analyses with increases in the presence and magnitude of autocorrelation from 8.50 to
666 $597.5 \text{ m}^3/\text{s}$ and then subsequent decline with increasing flow (Figure 9A). At the lowest
667 discharge there are approximately two broad bands of positive autocorrelation that
668 exceeded both the white noise and AR1 threshold at lag distances of 1400 and 2100 m .
669 At $28.32 \text{ m}^3/\text{s}$ these three peaks broaden and the highest correlation was found at lag
670 distance 1400 m , which increased from ~ 0.4 to 0.7 . At the bankfull discharge of 141.6
671 m^3/s the peak at 1400 m diminishes, while the peak near 2100 m increased in strength
672 (e.g. correlation magnitude). At $283.2 \text{ m}^3/\text{s}$ there are still peaks near 1400 and 2100
673 m that exceed both white noise and the AR1 threshold, but two other significant peaks
674 emerge near 700 and 2800 m . Similar statistically significant correlations are found at
675 $596.5 \text{ m}^3/\text{s}$, albeit narrower bands of correlation. The correlation distances at 283.2 and
676 $596.5 \text{ m}^3/\text{s}$ average $\sim 700 \text{ m}$, and this would have a frequency of approximately 0.0014
677 cycles/m . Beyond $596.5 \text{ m}^3/\text{s}$ the ACF diminishes rapidly with no peaks that are
678 statistically significant compared to red noise. Overall, the ACF results show that

679 $C(Z, W^j)$ is quasi-periodic from 8.50 m³/s to 141.6-597.5 m³/s, but then the periodicity
680 decreases in strength as flow increased.

681 Similar to ACF analysis, PSD analysis showed quasi-periodic components of
682 $C(Z, W^j)$ exhibiting flow dependent behavior (Figure 9B). For 8.50-283.2 m³/s there is a
683 high power band (e.g. PSD/ σ ~12-16) centered on 0.0014 cycles/m, which is confirmed
684 from the ACF analysis above. For 8.50 -141.6 m³/s there are also smaller magnitude
685 peaks ranging from 3-8, spread out over several frequencies. There's also a high
686 magnitude component at the lowest frequency band that emerges at 28.32 and declines
687 by 283.2 m³/s. These low frequency components are commonly associated with first
688 order auto-regressive behavior in the data (Shumway and Stoffer, 2010). At 597.5 m³/s
689 power is still associated on 0.0014 cycles/m, albeit with a ~50% reduction in magnitude.
690 Beyond this flow the frequency range and magnitude of statistically significant values
691 declines with discharge. Overall, both ACF and PSD results show that $C(Z, W^j)$ is
692 quasi-periodic from 8.50 m³/s to 283.2 m³/s but then decreased in strength as flow
693 increased. Further, the PSD results show that the $C(Z, W^j)$ GCS is flow dependent and
694 multiscalar, being characterized by a range of statistically significant frequencies.

695

696 **6. Discussion**

697 *6.1 Coherent undulations in cobble-gravel bed river topography*

698 The primary result of this study is that in an incising, partly confined, regulated
699 cobble-gravel river whose flow regime is dynamic enough to afford it the capability to
700 rejuvenate its landforms, there was a tendency for positive $C(Z, W^j)$ and thus covarying
701 Z and W^j amongst all flows analyzed. Based on the ACF and PSD analyses the

702 $C(Z, W^j)$ GCS undulations are quasi-periodic. The results of this study associated
703 channel organization across a range of recurrence intervals frequencies within the
704 range of commonly reported channel forming discharges for Western U.S. rivers (e.g.,
705 1.2-2.5 years) as well as substantially larger flows. These conclusions are obviously
706 limited to the study reach, but this should not prohibit discussing possible mechanisms
707 that could lead to these observed patterns, as well as the role of variable flows and
708 incision.

709 Most notably, the test river exhibited a dominance of covarying values of Z and
710 W^j across all flows, being characterized by an quasi-periodic pattern of wide and
711 shallow or narrow and deep cross sections. This supports the idea that alluvial river
712 reaches have a tendency for adapting wide and shallow and narrow and deep cross
713 sections to convey water flow (Huang et al., 2004). Rather than select a single type of
714 cross section to maximize energy dissipation to create a uniform cross section geometry
715 at a single channel maintaining flow, commonly referred to as bankfull, it appears that
716 alluvial rivers adjust their channel topography to have cross sections that roughly
717 alternate between those that are wide and shallow and narrow and deep (Figure 6B;
718 Huang et al., 2004), with some locations having a prismatic channel form indicative of
719 normative conditions, particularly in transition zones. Whether this is attributed to
720 minimizing the time rate of potential energy expenditure per unit mass within a reach
721 (Langbein and Leopold, 1962; Yang, 1971; Cherkauer, 1973; Wohl et al., 1999) or
722 channel unit scale mechanisms associated with riffle-pool maintenance (Wilkinson et al.
723 2004; MacWilliams et al., 2006; Caamano et al., 2009; Thompson, 2010;) remains to be
724 determined. Given that extremal hypotheses and riffle-pool maintenance act at different,

725 yet interdependent scales, it is likely that both play an intertwined and inseparable role
726 in channel form. That said, extremal theories are limited to predicting mean channel
727 conditions within a reach (Huang et al., 2014), with no models that can yet fully predict
728 sub-reach scale alluvial river topography, so we turn our attention to more tractable
729 hydrogeomorphic processes related to the maintenance of riffle and pool topography.

730 Presumably, the quasi-oscillatory $C(Z, W^j)$ GCS pattern is also linked to flow
731 dependent patterns of convective acceleration and deceleration zones (Marquis and
732 Roy, 2011; MacVicar and Rennie, 2012), as the length scales of the GCS were aligned
733 with the spacing of erosional and depositional landforms such as bars and pools. This
734 aspect is supported by ACF and PSD results as well as other two studies on the test
735 reach. First, it appears that the quasi-periodicity of the $C(Z, W^j)$ GCS is related to the
736 pool-riffle oscillation in the river corridor. The PSD analysis showed that the dominant
737 frequency of $C(Z, W^j)$ was ~ 0.0014 cycles/m, which equates to a length scale of ~ 700
738 m (Figure 9). Three of the morphologic units (MUs) studied by Wyrick and Pasternack
739 (2014) can be used for context including pools, riffles, and point bars. In their results for
740 the Timbuctoo Bend Reach, pools, riffles, and point bars had an average frequency of
741 0.0029, 0.0028, and 0.001 cycles/m. Considering that pools and riffles are defined as
742 two end-members of positive $C(Z, W^j)$, then the frequency of riffles and pools should be
743 twice that of the $C(Z, W^j)$ GCS as found herein. That is, a single oscillation of $C(Z, W^j)$
744 GCS would include both a narrow and deep (e.g. pool) and a wide and shallow (e.g.
745 riffle) cross section geometry, although transitional forms are possible within a cycle, too
746 (Figure 3). Therefore, it appears that the quasi-periodicity of the $C(Z, W^j)$ GCS is related
747 to the pool-riffle oscillation in the river corridor. This is in agreement with studies based

748 on field investigations and numerical models that relate this observation to quasi-
749 periodic bed and width variations associated with bar-pool topography (Richards,
750 1976b; Repetto and Tubino, 2001; Carling and Orr, 2002).

751 Second, Sawyer et al. (2010) showed that stage dependent flow convergence
752 maintained bed relief by topographically mediated changes in peak velocity and shear
753 stress at the central riffle in second example (Figure 5). Interestingly, the flow width
754 series phases relative to bed elevations in accordance with theory (Wilkinson et al.,
755 2004) and field and numerical studies (Brown and Pasternack, 2014). This supports an
756 already reported relationship between the $C(Z, W^j)$ GCS and the process of flow
757 convergence routing (Brown and Pasternack, 2014 Brown et al., 2016).

758 Lastly, Strom and Pasternack (2016) showed that peak zones of velocity undergo
759 variable changes in their location with discharge, with most velocity reversals occurring
760 after $597.5 \text{ m}^3/\text{s}$. In this case the zones of peak velocity patches underwent complex
761 changes from being associated with narrow topographic high points at base flows
762 $(-W^j, +Z)$ to topographic low points where flow width is constricted at high flows
763 $(-W^j, -Z)$. Overall, the presence of oscillating wide and shallow and narrow and deep
764 cross sections appears to be linked to hydrogeomorphic processes of riffle-pool
765 maintenance.

766

767 6.2 Hierarchical nesting, variable flows and the role of incision

768 This study quantitatively supports the idea that river morphology in partially confined
769 valleys is hierarchically nested with broader exogenic constraints such as the bedrock
770 valley walls, as well as channel width scale alluvial controls such as point bars and

771 islands. Our study quantitatively characterized interesting shifts in the amount of
772 correlation amongst flow width series and in the presence of quasi-periodic oscillations
773 in $C(Z, W^j)$ with changes in flow. Each series of W^j were significantly correlated with
774 the next highest flow, but this was lowest between 597.5 and 1195 m³/s, where the
775 valley walls begin to be engaged (Figure 7). Further, both the ACF and PSD show that
776 quasi-periodicity in $C(Z, W^j)$ declines after 597.5 m³/s (Figure 9). In addition, Strom and
777 Pasternack (2016) showed that reversals in peak velocity occur when flows exceed
778 597.5 m³/s. While results show that statistically significant correlations between Z and
779 W^j occur for a range of flows, the greatest magnitude is not when the valley walls are
780 inundated, but for the 283.2 m³/s channel and incipient floodplain. Given that
781 correlations were still significant for the flows that inundate the valley walls, this does
782 not refute the role of valley width oscillations in potentially controlling riffle persistence
783 (White et al., 2010), but rather adds new insight to the morphodynamics of rivers
784 incising in partially confined valleys. This suggests that the incision process may be
785 decoupling the organization of the riverbed away from being controlled by the valley
786 walls and instead phased towards reshaping channel topography within the inset bars
787 that are nested within the valley walls. As the riverbed incises further down through
788 knickpoint migration (Carley et al., 2012) this may act to shift zones of high and low
789 wetted width upstream unless lateral erosion can keep pace.

790

791 6.3 *Broader Implications*

792 This study quantified relationships between flow width and minimum bed elevation in
793 a partly confined and incising gravel-cobble bedded river, as well as for the first time

794 how they change with stage. While study results are currently limited to rivers similar to
795 the study reach, there are several key results of this study that may have broader
796 relevance to river restoration and management.

797 First, a key result of this study was that channel geometry was organized into
798 covarying Z and W^j undulations across all flows analyzed, alternating between wide and
799 shallow and narrow and deep cross sections. This is a very different view from the
800 classical definition of singular and modal bankfull channel geometry often used to guide
801 river and stream restoration (Shields et al., 2003). Instead, our study found that channel
802 geometry at all flows had a relatively even mixture of wide and shallow and narrow and
803 deep cross sections. Studies that deconstruct the complexity of river channel geometry
804 to modal ranges of channel width and depth have always shown scatter, which has
805 mostly been attributed to measurement uncertainty and/or local conditions (Park, 1977;
806 Philips and Harman, 1984; Harman et al., 2008; Surian et al., 2009). Our study
807 suggests that this variability is a fundamental component of alluvial river geometry.
808 While this concept was proposed by Hey and Thorne (1983) over two decades ago, few
809 studies have integrated these ideas into river engineering and design (e.g. see Simon et
810 al., 2007). Thus, this study further supports a needed shift away from designing rivers
811 with modal conditions to designing rivers with quasi-oscillatory and structured variations
812 in channel topography. An example of this is the form-process synthesis of channel
813 topography that experience flow reversals using GCS theory (Brown et al., 2016)

814 Second, this study has implications to restoration design and flow reregulation in that
815 a wide array of discharges beyond a single channel forming flow are presumably
816 needed for alluvial channel maintenance (Parker et al., 2003). Commonly singular

817 values of channel forming discharge, usually either bankfull or effective discharge, are
818 used in stream and river restoration designs (Shields et al., 2007; Doyle et al., 2007).
819 This study refutes this concept for rivers such as studied herein, as supported by the
820 results that show gradual changes in channel organization within a band of discharges
821 with recurrence intervals ranging from 1.2-5 years, and four fold range in absolute
822 discharges. Instead, stream and river restoration practitioners should analyze ranges of
823 flow discharges and the potential topographic features (existing or designed) that could
824 invoke stage-dependent hydrodynamic and geomorphic processes associated with
825 complex, self maintaining natural rivers.

826 Third, while the length scales of covarying Z and W^j undulations are approximate to
827 the spacing of bars and pools in the study area, they are quite complex and lack explicit
828 cutoffs that illustrate power in a singular frequency band. Thus, river restoration efforts
829 that specify modal values of bedforms may overly simplify the physical structure of
830 rivers with unknown consequences to ecological communities and key functions that are
831 the focus of such efforts. River restoration designs need to mimic the multiscalar nature
832 of self-formed topography by incorporating GCS into river engineering (Brown et al.,
833 2014) or somehow insure that simpler uniscalar designs will actually evolve into
834 multiscalar ones given available flows and anthropogenic boundary constraints.

835 Fourth, this study has potential implications for analyzing the effect of flow
836 dependent responses to topography and physical habitat in river corridors. Valley and
837 channel widths have shown to be very predictive in predicting the intrinsic potential of
838 salmon habitat (Burnett et al., 2007). Further, the role of covarying bed and width
839 undulations in modulating velocity signals and topographic change has implications to

840 the maintenance of geomorphic domains used by aquatic organisms. As one example,
841 consider that adult salmonids use positively covarying zones such as riffles (e.g.
842 $+W^j, +Z$) for spawning and pools (e.g. $-W^j, -Z$) for holding (Bjorn and Reiser, 1991). In
843 the study reach Pasternack et al. (2014) showed that 77% of spawning occurred in
844 riffles and chute morphologic units, which are at or adjacent to areas where $C(Z, W^j) > 1$
845 (Figure 4, Figure 5), supporting this idea. The presence and structure of covarying bed
846 and width undulations is also thought to be important indirectly for juvenile salmonids
847 that require shallow and low velocity zones for refugia during large floods. For example,
848 the expansions that occur at the head of riffles would presumably provide lateral zones
849 of shallow depths and moderate velocities needed for flood refugia. In the absence of
850 positive bed relief, and zones of $+W, +Z$, flow refugia zones would be hydrologically
851 disconnected from overbank areas, impacting the ability of juvenile salmon to utilize
852 these areas as refugia during floods and potentially leading to population level declines
853 (Nickelson et al., 1992). Future work should better constrain the utility of GCS concepts
854 in assessing aquatic habitat.

855 Lastly, it is possible that the $C(Z, W^j)$ GCS could be used as a comparative proxy in
856 remote sensing applications to determine how the topographic structure of rivers
857 change with flow, and how that may also change through time. The zoomed examples
858 of $C(Z, W^j)$ and the detrended river topography highlight how this type of GCS can be
859 used to characterize the topographic influence on wetted width and bed elevation
860 variability in river corridors. The $C(Z, W^j)$ GCS may be used diagnostically to assess
861 riverine structure and hydraulic function in a continuous manner within a river across an
862 array of flows. While not studied herein, prior work (Brown and Pasternack, 2014)

863 showed that the magnitude of $C(Z, W^j)$ can also be related to flow velocity, though
864 lagged effects do occur. Since the magnitudes can be linked to both unique landforms
865 and flow velocity they may have utility in assessing topographic and hydraulic controls
866 in river corridors.

867 LiDAR and analytical methods for developing bed topography in rivers has improved
868 considerably (McKean et al, 2009). For example, Gessese et al. (2011) derived an
869 analytical expression for determining bed topography from water surface elevations,
870 which can be obtained from LiDAR (Magirl et al, 2005). Assuming one has an adequate
871 topographic data set, whether numerical flow modeling is needed to generate wetted
872 width data sets places a considerable constraint on performing this type of analysis.
873 This could potentially be relaxed, especially at flows above bankfull, using a constant
874 water slope approximation for various flow stages. At smaller discharges in rivers there
875 are typically defects in the water surface elevation, where the bed topography exerts a
876 strong control on bed elevations (e.g. Brown and Pasternack, 2008). However, many
877 studies suggest that on large alluvial rivers bankfull and flood profiles show that they
878 generally flatten and smoothen once bed forms and large roughness elements such as
879 gravel bars are effectively submerged. In this case, one can then detrend the river
880 corridor and take serial width measurements associated at various heights above the
881 riverbed (Gangodagamage et al., 2007). The height above the river then can then be
882 related to estimates of flow discharge and frequency, so that the change GCS structure
883 can be related to watershed hydrology (Jones, 2006). There's also the obvious option of
884 using paired aerial photography with known river flows by correlating discharge with
885 imagery dates and widths. Future work should constrain whether similar conclusions

886 can be reached using field and model derived estimates of wetted width as opposed to
887 modeled solutions.

888

889 **7. Conclusions**

890 A key conclusion is that the test river exhibited covarying oscillations of minimum bed
891 elevation and channel top width across all flows analyzed. These covarying oscillations
892 were found to be quasi-periodic at channel forming flows, scaling with the length scales
893 of pools and riffles. Thus it appears that alluvial rivers organize their topography to
894 have oscillating shallow and wide and narrow and deep cross section geometry, even
895 despite ongoing incision. Presumably these covarying oscillations are linked to
896 hydrogeomorphic mechanisms associated with alluvial river channel maintenance. As
897 an analytical tool, the GCS concepts in here treat the topography of river corridors as
898 system, which is thought of as an essential view in linking physical and ecological
899 processes in river corridors at multiple scales (Fausch et al., 2002; Carbonneau et al.,
900 2012). While much research is needed to validate the utility of these ideas to these
901 broader concepts and applications in ecology and geomorphology, the idea of GCS's,
902 especially for width and bed elevation, holds promise.

903

904 **8. Data Availability**

905 Each $C(Z, W^j)$ dataset is available from either author by request.

906

907 **9. Acknowledgements**

908 Although not directly funded by any source, this study used data and models

909 from studies previously sponsored by Pacific Gas & Electric Company, the U.S. Fish
910 and Wildlife Service Anadromous Fish Restoration Program, Yuba County Water
911 Agency, and the Yuba Accord River Management Team. Co-author G.B. Pasternack
912 received support from the USDA National Institute of Food and Agriculture, Hatch
913 project number #CA-D-LAW-7034-H.

914

915 **10. References**

916 Abu-Aly TR, Pasternack GB, Wyrick JR, Barker R, Massa D, Johnson T. 2014. Effects
917 of LiDAR-derived, spatially distributed vegetation roughness on two-dimensional
918 hydraulics in a gravel-cobble river at flows of 0.2 to 20 times bankfull.
919 *Geomorphology* 206: 468-482. DOI: 10.1016/j.geomorph.2013.10.017

920 Adler, LL. 1980. Adjustment of Yuba River, California, to the influx of hydraulic mining
921 debris, 1849–1979. M.A. thesis, Geography Department, University of California,
922 Los Angeles.

923 Andrews ED. 1980. Effective and bankfull discharges of streams in the Yampa River
924 basin, Colorado and Wyoming. *Journal of Hydrology* 46: 311-330.

925 Bjorn TC, Reiser DW. 1991 Habitat Requirements of Salmonids in Streams. In:
926 Influences of Forest and Rangeland Management on Salmonid Fishes and Their
927 Habitats. Edited by W.R. Meehan. Special Publication 19. American Fisheries
928 Society. Bethesda, MD. pp. 83-138.

929 Brown RA. 2014. The Analysis and Synthesis of River Topography (Doctoral
930 Dissertation) University Of California, Davis. 187 pages.

931 Brown RA, Pasternack, GB. 2008. Engineered channel controls limiting spawning
932 habitat rehabilitation success on regulated gravel-bed rivers. *Geomorphology* 97:
933 631–654.

934 Brown RA, Pasternack GB. 2014. Hydrologic and Topographic Variability Modulate
935 Channel Change in Mountain Rivers. *Journal of Hydrology* 510: 551–564. DOI:
936 10.1016/j.jhydrol.2013.12.048

937 Brown, R.A., Pasternack, G.B., Wallender, W.W., 2014. Synthetic River Valleys:
938 Creating Prescribed Topography for Form-Process Inquiry and River
939 Rehabilitation Design. *Geomorphology* 214.

- 940 Brown, R.A., Pasternack, G.B., Lin, T., 2016. The topographic design of river channels
941 for form-process linkages. *Environmental Management*, 57(4), 929-942.
- 942 Burnett KM, Reeves GH, Miller DJ, Clarke S, Vance-Borland K, and Christiansen K.
943 2007. Distribution Of Salmon-Habitat Potential Relative To Landscape
944 Characteristics And Implications For Conservation. *Ecological Applications*
945 17:66–80.[http://dx.doi.org/10.1890/10510761\(2007\)017\[0066:DOSPRT\]2.0.CO;2](http://dx.doi.org/10.1890/10510761(2007)017[0066:DOSPRT]2.0.CO;2)
- 946 Caamaño D, Goodwin P, Buffington JM. 2009. Unifying criterion for the velocity reversal
947 hypothesis in gravel-bed rivers. *Journal of Hydraulic Engineering* 135: 66–70.
- 948 Carbonneau P, Fonstad MA, Marcus WA, Dugdale SJ. 2012. Making riverscapes real.
949 *Geomorphology*. 137:74-86. DOI: 10.1016/j.geomorph.2010.09.030
- 950 Carley JK, Pasternack GB, Wyrick JR, Barker JR, Bratovich PM., Massa D, Reedy G, ,
951 Johnson TR. 2012. Significant decadal channel change 58–67years post-dam
952 accounting for uncertainty in topographic change detection between contour
953 maps and point cloud models. *Geomorphology* 179: 71-88. DOI:
954 10.1016/j.geomorph.2012.08.001
- 955 Carling PA, Orr HG. 2000. Morphology of riffle-pool sequences in the River Severn,
956 England. *Earth Surface Processes and Landforms* 25: 369–384. DOI:
957 10.1002/(SICI)1096-9837(200004)25:4<369::AID-ESP60>3.0.CO;2-M
- 958 Carter G, Knapp C, Nuttall A. 1973. Estimation of the magnitude-squared coherence
959 function via overlapped fast Fourier transform processing. *IEEE Transactions on*
960 *Audio and Electroacoustics* 21: 337 – 344. DOI: 10.1109/TAU.1973.1162496
- 961 Cherkauer DS. 1973. Minimization of power expenditure in a riffle-pool alluvial channel.
962 *Water Resources Research* 9: 1613–1628.
- 963 Cienciala P, Pasternack, GB. in press. Floodplain Inundation Response to Climate,
964 Valley Form, and Flow Regulation on a Gravel-Bed River in a Mediterranean-
965 Climate Region. *Geomorphology*.
- 966 . Church, M, 2006. Multiple scales in rivers, In: Helmut Habersack, Hervé Piégay and
967 Massimo Rinaldi, Editor(s), *Developments in Earth Surface Processes*, Elsevier,
968 2007, Volume 11, Pages 3-28, ISSN 0928-2025, ISBN 9780444528612,
969 [http://dx.doi.org/10.1016/S0928-2025\(07\)11111-](http://dx.doi.org/10.1016/S0928-2025(07)11111-1)
970 1.(<http://www.sciencedirect.com/science/article/pii/S0928202507111111>)
- 971 Colombini M, Seminara G, Tubino M. 1987. Finite-amplitude alternate bars. *Journal of*
972 *Fluid Mechanics* 181: 213-232. DOI: 10.1017/S0022112087002064

- 973 Cox N, J. 1983. On the estimation of spatial autocorrelation in geomorphology. *Earth*
974 *Surface Processes and Landforms* 8: 89–93. DOI: 10.1002/esp.3290080109
- 975 Davis, W.M., 1909. *The Geographical Cycle*, Chapter 13, *Geographical Essays*. Ginn
976 and Co., New York.
- 977 DeAlmeida GAM, Rodriguez JF. 2012. Spontaneous formation and degradation of pool-
978 riffle morphology and sediment sorting using a simple fractional transport model.
979 *Geophysical Research Letters* 39, L06407, doi:10.1029/2012GL051059.
- 980 Dolan R, Howard A, Trimble D. 1978. Structural control of the rapids and pools of the
981 Colorado River in the Grand Canyon. *Science* 10: 629-631. DOI:
982 10.1126/science.202.4368.629
- 983 Doyle MW, Shields D, Boyd KF, Skidmore PB, Dominick D. 2007. Channel-Forming
984 Discharge Selection in River Restoration Design. *Journal of Hydraulic*
985 *Engineering* 133(7):831-837.
- 986 Escobar-Arias MI, Pasternack G.B. 2011. Differences in River Ecological Functions Due
987 to Rapid Channel Alteration Processes in Two California Rivers Using the
988 Functional Flows Model, Part 2- Model Applications. *River Research and*
989 *Applications* 27, 1–22, doi: 10.1002/rra.1335.
- 990 Frissell CA, Liss WJ, Warren CE, Hurley MD. 1986. A hierarchical framework for stream
991 habitat classification: Viewing streams in a watershed context. *Environmental*
992 *Management* 10(2): 199-214.
- 993 Gangodagamage, C, Barnes, E, Fofoula Georgiou, E. 2007. Scaling in river corridor
994 widths depicts organization in valley morphology, *Geomorphology*, 91, 198–215,
995 doi:10.1016/j.geomorph.2007.04.014.
- 996 Gessese AF, Sellier M, Van Houten E, Smart, G. 2011. Reconstruction of river bed
997 topography from free surface data using a direct numerical approach in one-
998 dimensional shallow water flow. *Inverse Problems* 27.
- 999 Gilbert GK, 1917. *Hydraulic-mining debris in the Sierra Nevada*. United States
1000 Geological Survey Professional Paper 105.
- 1001 Ghoshal S, James LA, Singer MB, Aalto R. 2010. Channel and Floodplain Change
1002 Analysis over a 100-Year Period: Lower Yuba River, California. *Remote Sensing*,
1003 2(7): 1797.
- 1004 Guinn JM. 1890. Exceptional years: a history of California floods and drought. *Historical*
1005 *Society of Southern California* 1 (5): 33-39.

- 1006 Harman C, Stewardson M, DeRose R. 2008. Variability and uncertainty in reach
1007 bankfull hydraulic geometry. *Journal of Hydrology* 351(1-2):13-25, ISSN 0022-
1008 1694, <http://dx.doi.org/10.1016/j.jhydrol.2007.11.015>.
- 1009 Harrison LR, Keller EA. 2007. Modeling forced pool–riffle hydraulics in a boulder-bed
1010 stream, southern California. *Geomorphology* 83: 232–248. DOI:
1011 10.1016/j.geomorph.2006.02.024
- 1012 Hernandez G. 1999. Time series, periodograms, and significance, *J. Geophys. Res.*,
1013 104(A5), 10355–10368, doi:10.1029/1999JA900026.
- 1014 Hey RD, Thorne CR. 1986. Stable channels with mobile gravel beds. *Journal of*
1015 *Hydraulic Engineering* 112: 671–689.
- 1016 Huang HQ, Chang HH, Nanson GC. 2004. Minimum energy as the general form of
1017 critical flow and maximum flow efficiency and for explaining variations in river
1018 channel pattern, *Water Resour. Res.*, 40, W04502, doi:10.1029/2003WR002539.
- 1019 Huang HQ, Deng C, Nanson GC, Fan B, Liu X, Liu T, Ma Y. 2014. A test of equilibrium
1020 theory and a demonstration of its practical application for predicting the
1021 morphodynamics of the Yangtze River. *Earth Surf. Process. Landforms*, 39: 669–
1022 675.
- 1023 Jackson JR, Pasternack GB, Wyrick JR. 2013. Substrate of the Lower Yuba River.
1024 Prepared for the Yuba Accord River Management Team. University of California,
1025 Davis, CA, 61pp.
- 1026 James LA, Singer MB, Ghoshal S. 2009. Historical channel changes in the lower Yuba
1027 and Feather Rivers, California: Long-term effects of contrasting river-
1028 management strategies. *Geological Society of America Special Papers* 451:57-
1029 81. DOI: 10.1130/2009.2451(04)
- 1030 Keller E. 1971. Areal Sorting of Bed-Load Material: The Hypothesis of Velocity
1031 Reversal. *Geological Society of America Bulletin* 82: 753-756.
- 1032 Keller EA, Melhorn WN. 1978. Rhythmic spacing and origin of pools and riffles: *GSA*
1033 *Bulletin* 89: 723-730. DOI: 10.1130/0016-7606(1978)89<723:RSAOOP>2.0.CO;2
- 1034 Knighton A. 1983. Models of stream bed topography at the reach scale. *Journal of*
1035 *Hydrology* 60.
- 1036 Lisle, T 1979. A Sorting Mechanism For A Riffle-Pool Sequence. *Geological Society of*
1037 *America Bulletin*, Part 11. 90: 1142-1157.

- 1038 Leopold LB, Maddock T. 1953. The Hydraulic Geometry of Stream Channels and Some
1039 Physiographic Implications. Geological Survey Professional Paper 252, United
1040 States Geological Survey, Washington, D.C.
- 1041 Leopold, LB and Langbein, WB. 1962. The Concept of Entropy in Landscape Evolution,
1042 U.S. Geological Survey Professional Paper 500-A, 20p.
- 1043 MacWilliams, ML, Jr, Wheaton, JM, Pasternack, GB, Street, RL, Kitanidis, PK. 2006.
1044 Flow convergence routing hypothesis for pool–riffle maintenance in alluvial rivers.
1045 Water Resources Research 42, W10427. doi:10.1029/2005WR004391.
- 1046 Madej MA. 2001. Development of channel organization and roughness following
1047 sediment pulses in single-thread, gravel bed rivers. Water Resources Research
1048 37: 2259-2272. DOI: 10.1029/2001WR000229
- 1049 Magirl CS, Webb RH, Griffiths PG. 2005. Changes in the water surface profile of the
1050 Colorado River in Grand Canyon, Arizona, between 1923 and 2000, Water
1051 Resour. Res., 41, W05021, doi:10.1029/2003WR002519.
- 1052 MacVicar BJ, Rennie CD. 2012. Flow and turbulence redistribution in a straight artificial
1053 pool. Water Resources Research 48, W02503, doi:10.1029/2010WR009374
- 1054 Marquis GA, Roy AG. 2011. Bridging the gap between turbulence and larger scales of
1055 flow motions in rivers. Earth Surface Processes and Landforms 36: 563–568.
1056 doi:10.1002/esp.2131
- 1057 McKean JA, Isaac DJ, Wright CW. 2008. Geomorphic controls on salmon nesting
1058 patterns described by a new, narrow-beam terrestrial–aquatic lidar. Frontiers in
1059 Ecology and the Environment 6: 125-130. DOI: 10.1890/070109
- 1060 McKean J, Nagel D, Tonina D, Bailey P, Wright CW, Bohn,C, Nayegandhi A, 2009.
1061 Remote sensing of channels and riparian zones with a narrow-beam aquatic-
1062 terrestrial lidar. Remote Sensing, 1, 1065-1096; doi:10.3390/rs1041065.
- 1063 Melton MA. 1962. Methods for measuring the effect of environmental factors on channel
1064 properties. Journal of Geophysical Research 67: 1485-1490. DOI:
1065 10.1029/JZ067i004p01485
- 1066 Milan DJ, Heritage GL, Large ARG, Charlton ME. 2001. Stage dependent variability in
1067 tractive force distribution through a riffle-pool sequence. Catena 44: 85-109.
- 1068 Milne JA. 1982. Bed-material size and the riffle-pool sequence. Sedimentology 29: 267-
1069 278. DOI: 10.1111/j.1365-3091.1982.tb01723.x

- 1070 Nelson PA, Brew AK, Morgan, JA. 2015. Morphodynamic response of a variable-width
1071 channel to changes in sediment supply. *Water Resources Research* 51: 5717–
1072 5734, doi:10.1002/2014WR016806.
- 1073 Newland DE. 1993. An introduction to random vibrations, spectral and wavelet analysis.
1074 Dover Publications.
- 1075 Nickelson TA, Rodgers J, Steven L. Johnson, Mario F. Solazzi. 1992. Seasonal
1076 Changes in Habitat Use by Juvenile Coho Salmon (*Oncorhynchus kisutch*) in
1077 Oregon Coastal Streams. *Canadian Journal of Fisheries and Aquatic Sciences*,
1078 1992, 49:783-789, 10.1139/f92-088
- 1079 Nolan KM, Lisle TE, Kelsey HM. 1987. Bankfull discharge and sediment transport in
1080 northwestern California. In: R. Beschta, T. Blinn, G. E. Grant, F. J. Swanson, and
1081 G. G. Ice (ed.), *Erosion and Sedimentation in the Pacific Rim (Proceedings of the*
1082 *Corvallis Symposium, August 1987)*. International Association of Hydrological
1083 Sciences Pub. No. 165, p. 439-449.
- 1084 Parker G., Toro-Escobar CM, Ramey M, Beck S, 2003. The effect of floodwater
1085 extraction on the morphology of mountain streams. *Journal of Hydraulic*
1086 *Engineering*, 129(11): 885-895.
- 1087 Pasternack GB, Tu D, Wyrick JR. 2014. Chinook adult spawning physical habitat of the
1088 lower Yuba River. Prepared for the Yuba Accord River Management Team.
1089 University of California, Davis, CA, 154pp.
- 1090 Pasternack GB, Wyrick JR. in press. Flood-driven topographic changes in a gravel-
1091 cobble river over segment, reach, and unit scales. *Earth Surface Processes and*
1092 *Landforms*
- 1093 Park CC. 1977. World-wide variations in hydraulic geometry exponents of stream
1094 channels: An analysis and some observations, *Journal of Hydrology* 33(1): 133-
1095 146, ISSN 0022-1694, [http://dx.doi.org/10.1016/0022-1694\(77\)90103-2](http://dx.doi.org/10.1016/0022-1694(77)90103-2).
- 1096 Phillips PJ, Harlin JM. 1984. Spatial dependency of hydraulic geometry exponents in a
1097 subalpine stream, *Journal of Hydrology* 71(3): 277-283. ISSN 0022-1694,
1098 [http://dx.doi.org/10.1016/0022-1694\(84\)90101-X](http://dx.doi.org/10.1016/0022-1694(84)90101-X).
- 1099 Pike RJ, Evans I, Hengl T. 2008. Geomorphometry: A Brief Guide. In: *Geomorphometry*
1100 *- Concepts, Software, Applications*, Hengl, T. and Hannes I. Reuter (eds.), Series
1101 *Developments in Soil Science* vol. 33, Elsevier, pp. 3-33, ISBN 978-0-12-374345-
1102 9

- 1103 Rayburg SC, Neave M. 2008. Assessing morphologic complexity and diversity in river
1104 systems using three-dimensional asymmetry indices for bed elements, bedforms
1105 and bar units. *River Research and Applications* 24: 1343–1361. DOI:
1106 10.1002/rra.1096
- 1107 Rendell H, Alexander D. 1979. Note on some spatial and temporal variations in
1108 ephemeral channel form. *Geological Society of America Bulletin* 9: 761-772. DOI:
1109 10.1130/0016-7606(1979)90<761:NOSSAT>2.0.CO;2
- 1110 Repetto R, Tubino M, 2001. Topographic Expressions of Bars in Channels with Variable
1111 Width. *Phys. Chem. Earth (B)*, Vol. 26:71-76.
- 1112 Richards KS. 1976a. The morphology of riffle-pool sequences. *Earth Surface Processes*
1113 1: 71-88. DOI: 10.1002/esp.3290010108
- 1114 Richards KS. 1976b. Channel width and the riffle-pool sequence. *Geological Society of*
1115 *America Bulletin* 87: 883-890.
- 1116 Richards KS. 1979. Stochastic processes in one dimension: An introduction. *Concepts*
1117 *and Techniques In Modern Geography* No. 23. 30 pages.
- 1118 Richter BD, Braun DP, Mendelson MA, Master LL. 1997. Threats to Imperiled
1119 Freshwater Fauna. *Conservation Biology* 11: 1081–1093.
- 1120 Rosgen D, 1996. *Applied River Morphology (Wildland Hydrology, Pagosa Springs,*
1121 *Colorado)*. Wildland Hydrology, Pagosa Springs, CO.
- 1122 Salas JD. 1980. *Applied modeling of hydrologic time series. Applied modeling of*
1123 *hydrologic time series. Water Resources Publications. Littleton, Colorado.*
- 1124 Sawyer, AM, Pasternack GB, Moir HJ, Fulton AA. 2010. Riffle-pool maintenance and
1125 flow convergence routing confirmed on a large gravel bed river. *Geomorphology*,
1126 114: 143-160
- 1127 Schumm SA. 1971. Fluvial geomorphology: channel adjustment and river
1128 metamorphosis. In: Shen, H.W. (Ed.), *River Mechanics*. H.W. Shen, Fort Collins,
1129 CO, pp. 5-1–5-22.
- 1130 Shields D, Copeland R., Klingeman P, Doyle M, and Simon A. 2003. Design for Stream
1131 Restoration. *Journal of Hydraulic Engineering* 10.1061/(ASCE)0733-
1132 9429(2003)129:8(575), 575-584.
- 1133 Shumway RH, Stoffer DS. 2010. *Time series analysis and its applications: with R*
1134 *examples. Time series analysis and its applications: with R examples. 505*
1135 *pages. Springer US.*

- 1136 Simon AM, Doyle M, Kondolf M, Shields FD, Rhoads B, and McPhillips M. 2007. Critical
1137 Evaluation of How the Rosgen Classification and Associated “Natural Channel
1138 Design” Methods Fail to Integrate and Quantify Fluvial Processes and Channel
1139 Response. *Journal of the American Water Resources Association* 43(5):1117-
1140 1131. DOI: 10.1111 / j.1752-1688.2007.00091.x
- 1141 Strom MA, Pasternack GB, Wyrick JR. 2016. Reenvisioning velocity reversal as a
1142 diversity of hydraulic patch behaviors. *Hydrologic Processes*, doi:
1143 10.1002/hyp.10797.
- 1144 Surian N, Mao L, Giacomini M, and Ziliani L. 2009. Morphological effects of different
1145 channel-forming discharges in a gravel-bed river. *Earth Surface Processes and
1146 Landforms* 34: 1093–1107. doi:10.1002/esp.1798
- 1147 Thomson JR, Taylor MP, Fryirs KA, Brierley GJ. 2001. A geomorphological framework
1148 for river characterization and habitat assessment. *Aquatic Conservation-Marine
1149 and Freshwater Ecosystems*, 11(5), 373-389.
- 1150 Thompson DM. 2010. The velocity-reversal hypothesis revisited. *Progress in Physical
1151 Geography* 35: 123–132. DOI: 10.1177/0309133310369921
- 1152 Thornbury WD. 1954. *Principles of geomorphology*. John Wiley, New York.
- 1153 Trauth MH, Gebbers R, Marwan N, Sillmann E. 2006. *MATLAB recipes for earth
1154 sciences*. Springer
- 1155 Wolman MG, Gerson R. 1978. Relative Scales of Time and Effectiveness of Climate in
1156 Watershed Geomorphology. *Earth Surface Processes and Landforms* 3(2): 189-
1157 208.
- 1158 White JQ, Pasternack GB, Moir HJ. 2010. Valley width variation influences riffle–pool
1159 location and persistence on a rapidly incising gravel-bed river. *Geomorphology*
1160 121: 206–221. DOI: 10.1016/j.geomorph.2010.04.012
- 1161 Wilkinson SN, Keller RJ, Rutherford ID. 2004. Phase-shifts in shear stress as an
1162 explanation for the maintenance of pool–riffle sequences. *Earth Surface
1163 Processes and Landforms* 29: 737–753. DOI: 10.1002/esp.1066
- 1164 Williams GP. 1978. Bank-full discharge of rivers, *Water Resources Research* 14:1141–
1165 1154. doi:10.1029/WR014i006p01141.
- 1166 Wohl EE, Thompson DM, Miller AJ. 1999. Canyons with undulating walls, *Geological
1167 Society of America Bulletin* 111, 949–959.

- 1168 Wolman MG, Gerson R 1978 Relative scales of time and effectiveness of climate in
1169 watershed geomorphology. *Earth Surface. Processes and Landforms* 3: 189–
1170 208. doi:10.1002/esp.3290030207
- 1171 Wyrick JR, Pasternack GB. 2012. Landforms of the lower Yuba River. University of
1172 California, Davis.
- 1173 Wyrick JR, Pasternack GB. 2014. Geospatial organization of fluvial landforms in a
1174 gravel–cobble river: Beyond the riffle–pool couplet. *Geomorphology* 213: 48-65.
1175 DOI: 10.1016/j.geomorph.2013.12.040
- 1176 Wyrick JR, Pasternack GB. 2015. Revealing the natural complexity of topographic
1177 change processes through repeat surveys and decision-tree classification. *Earth*
1178 *Surface Processes and Landforms*, doi: 10.1002/esp.3854.
- 1179 Yalin, MS. 1977. *Mechanics of sediment transport*. Elsevier
- 1180 Yang CT. 1971. Potential Energy and Stream Morphology. *Water Resources Research*
1181 7. DOI: 10.1029/WR007i002p00311
- 1182 Yu B, Wolman MG. 1987. Some dynamic aspects of river geometry, *Water Resources*
1183 *Research* 23(3): 501–509. doi:10.1029/WR023i003p00501.

1184 **11. List of Figures**

1185 Figure 1. Regional and vicinity map of the lower Yuba River (A) and extent of study
1186 segment showing inundation extents predicted by the 2D model (B).

1187

1188 Figure 2. Raw bed profile (A) and flow width (B) series for 283.2 m³/s. After detrending
1189 and standardizing, values of Z (black line in C) and W (blue line in C) are multiplied
1190 together to compute $C(Z, W^j)$ (red line in C). The whole series of $C(Z, W^j)$ is the GCS

1191

1192 Figure 3. Conceptual key for interpreting $C(Z, W^j)$ geomorphic covariance structures

1193 (A). For quadrant 1 Z and W^j are both relatively high, so that implies wide and shallow

1194 areas associated with deposition. Conversely, in quadrant 2 Z is relatively low, but and

1195 W^j is relatively high, which implies deep and wide cross areas, which implies that these
1196 areas may have been scoured at larger flows. In quadrant 3 Z and W^j are both
1197 relatively low, so that implies narrow and deep areas associated with erosion. Finally, in
1198 quadrant 4 Z is relatively high and W^j is relatively low, so that implies narrow and
1199 topographically high areas. Prototypical channels and GCS with positive (B), and
1200 negative (C) $C(Z, W^j)$ colored according to (A).

1201
1202 Figure 4. Example section in the middle of the study area showing inundation extents
1203 (A). Below are plots of minimum bed elevation (B), flow widths for 8.50 m³/s, 283.2 m³/s,
1204 and 3,126 m³/s (C), and $C(Z, W^j)$ for the same flows. The aerial image is for a flow of
1205 21.29 m³/s on 9/28/2006.

1206
1207 Figure 5. Example section at the lower extent of the study area showing inundation
1208 extents (A). Below are plots of minimum bed elevation (B), flow widths for 8.50 m³/s,
1209 283.2 m³/s, and 3,126 m³/s (C), and $C(Z, W^j)$ for the same flows. The aerial image is for
1210 a flow of 21.29 m³/s on 9/28/2006.

1211
1212 Figure 6. Histogram of $C(Z, W^j)$ classified by positive and negative values as well as >
1213 and < 1 (A). Also shown is a histogram classified by quadrant (B). Both illustrate an
1214 overall tendency for $C(Z, W^j) > 0$ with increasing discharge and also illustrating an
1215 increasing tendency for positive values of $C(Z, W^j) > 1$ up until 283.2 m³/s after which it
1216 declines. Colors represent bin centered values.

1217

1218 Figure 7. Pearson's correlation coefficient for Z and W^j between each flow.

1219

1220 Figure 8. Pearson's correlation coefficient for sequential pairs of flow dependent wetted
1221 width series.

1222

1223 Figure 9. Autocorrelation (A) and PSD (B) of $C(Z, W^j)$ with increasing flow. For the
1224 ACF plot (A), only values exceeding white noise at the 95% level are shown and the red
1225 countor demarcates the 95% level for an AR1 process(red noise). For the PSD plot (B)
1226 only values exceeding white noise at the 95% level are shown.

1227

1228 Table 1. Flows analyzed and their approximate annual recurrence intervals.

1229

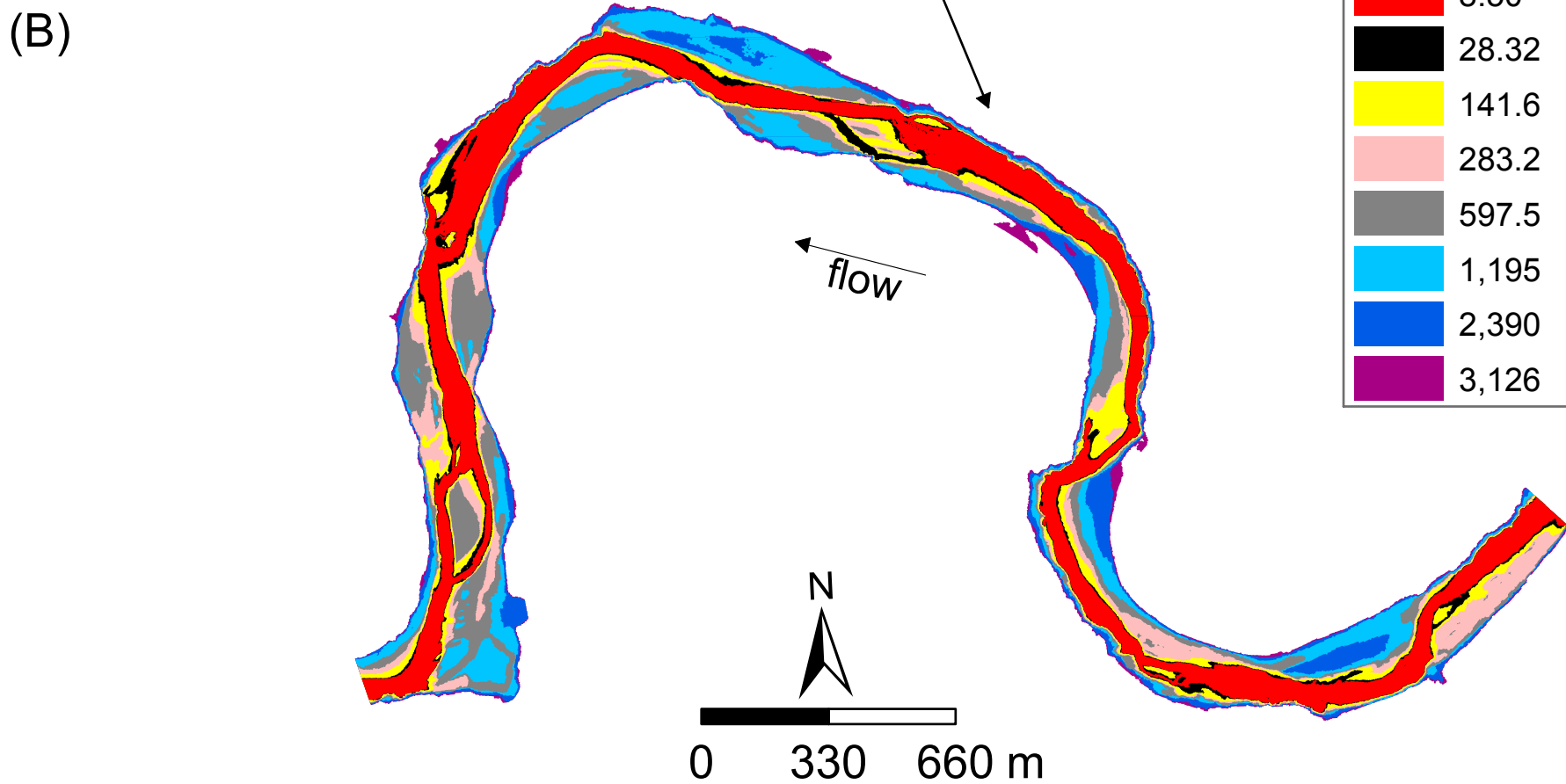
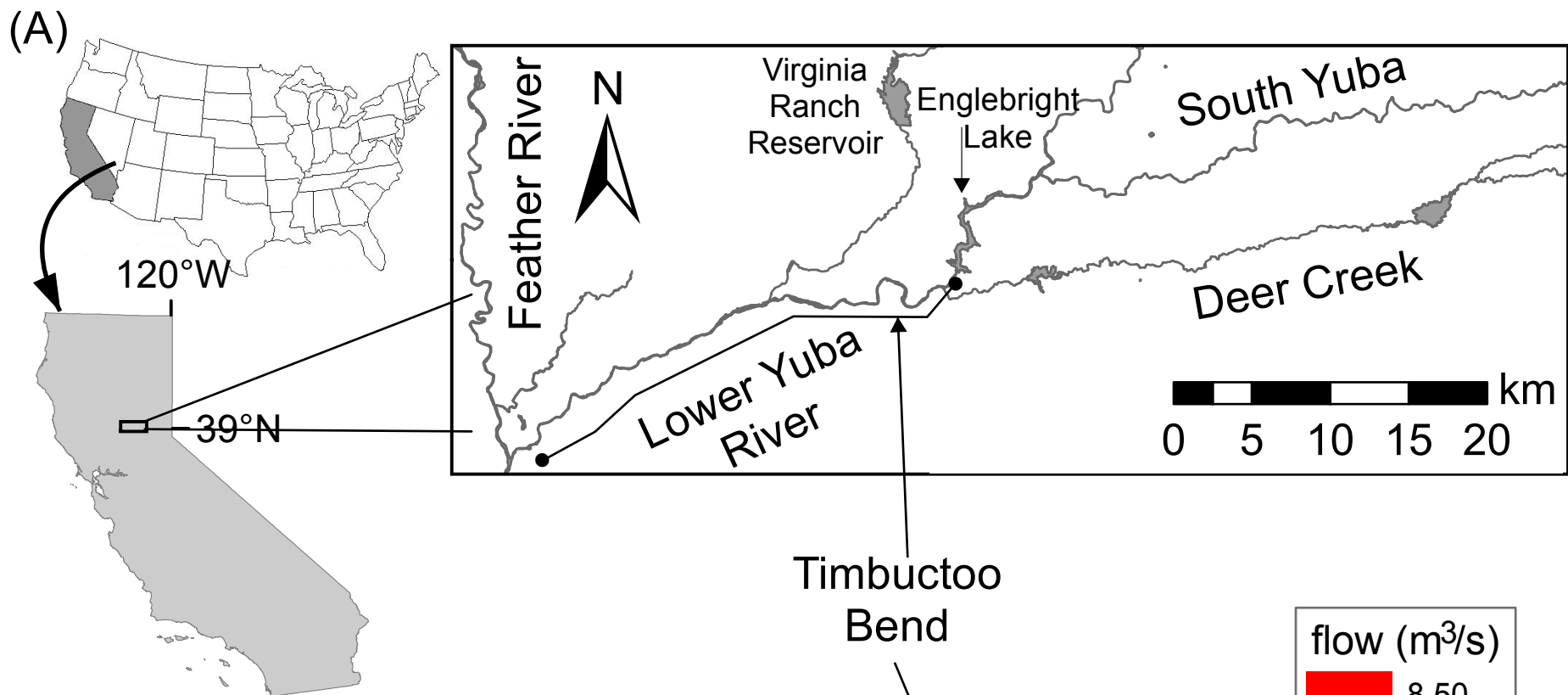
1230 Table 2. Linear trend models and R^2 for Z and W^j used in detrending each series.

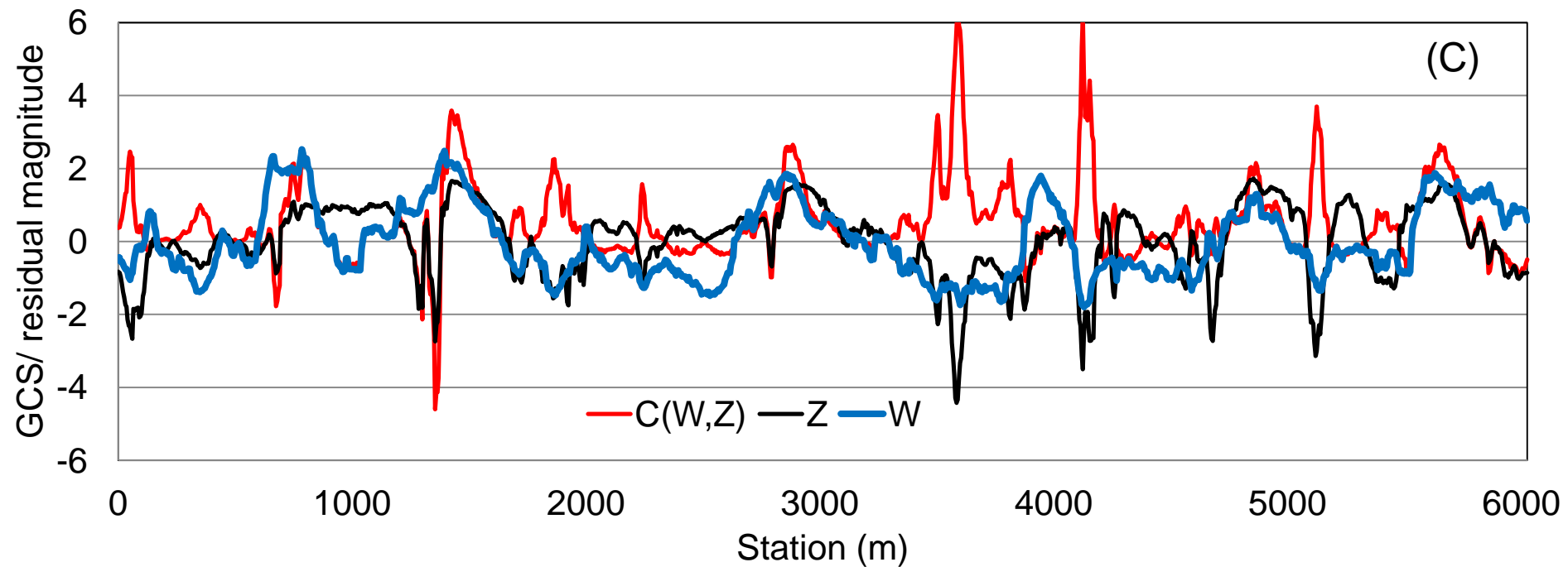
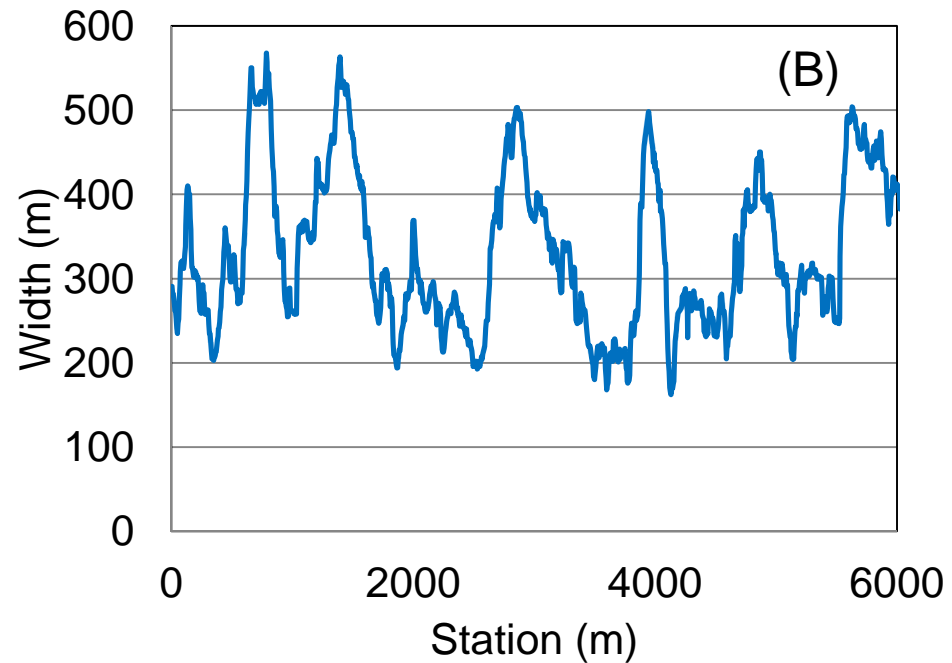
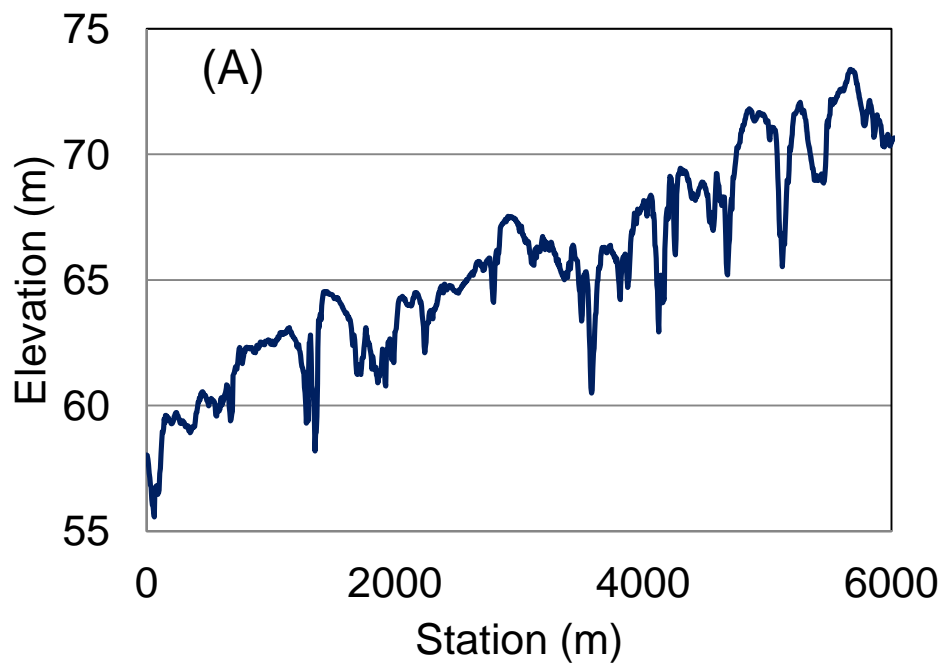
1231

1232 Table 3. Mann Whitney U-test p values amongst all combinations of Z and W^j at the
1233 95% level.

1234

1235





(A)

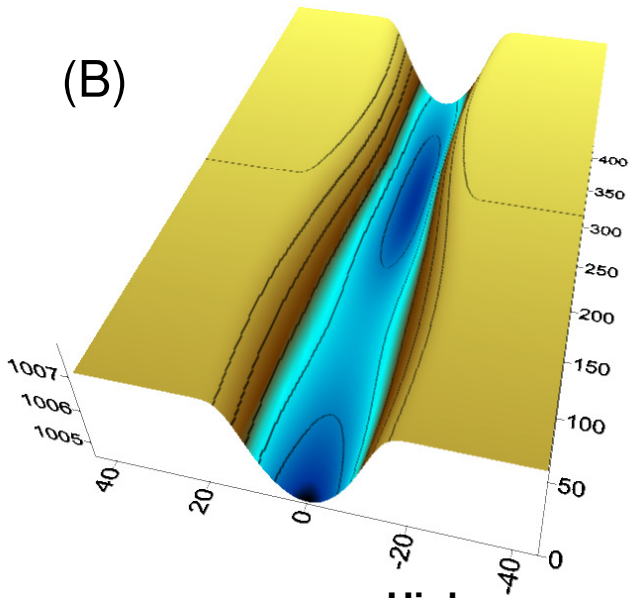
Relative Bed Elevation

 $-Z$ $+Z$

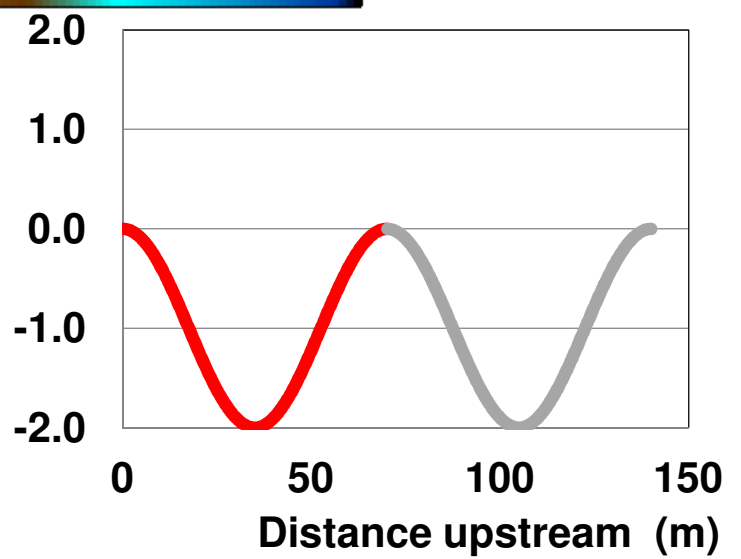
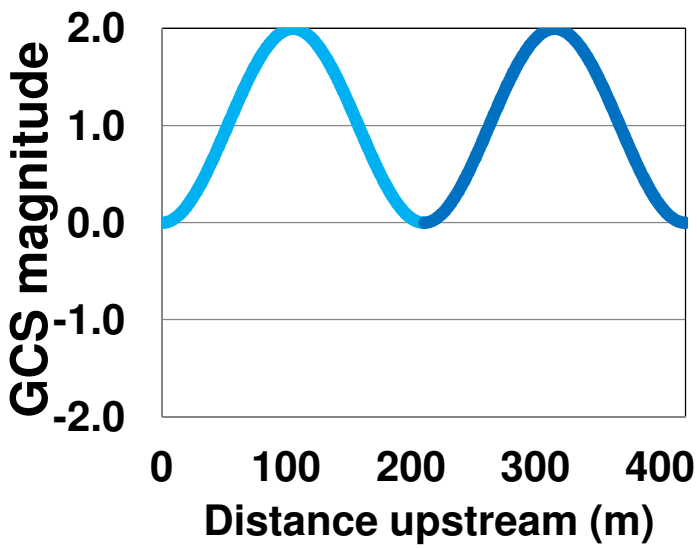
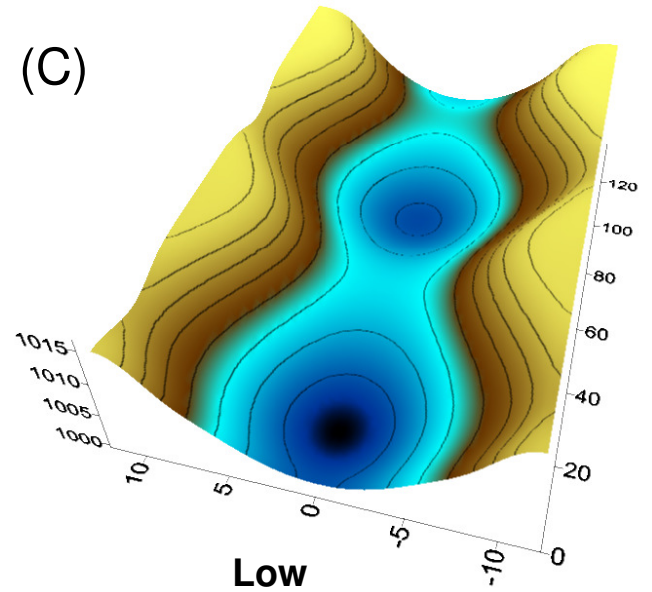
Relative Width

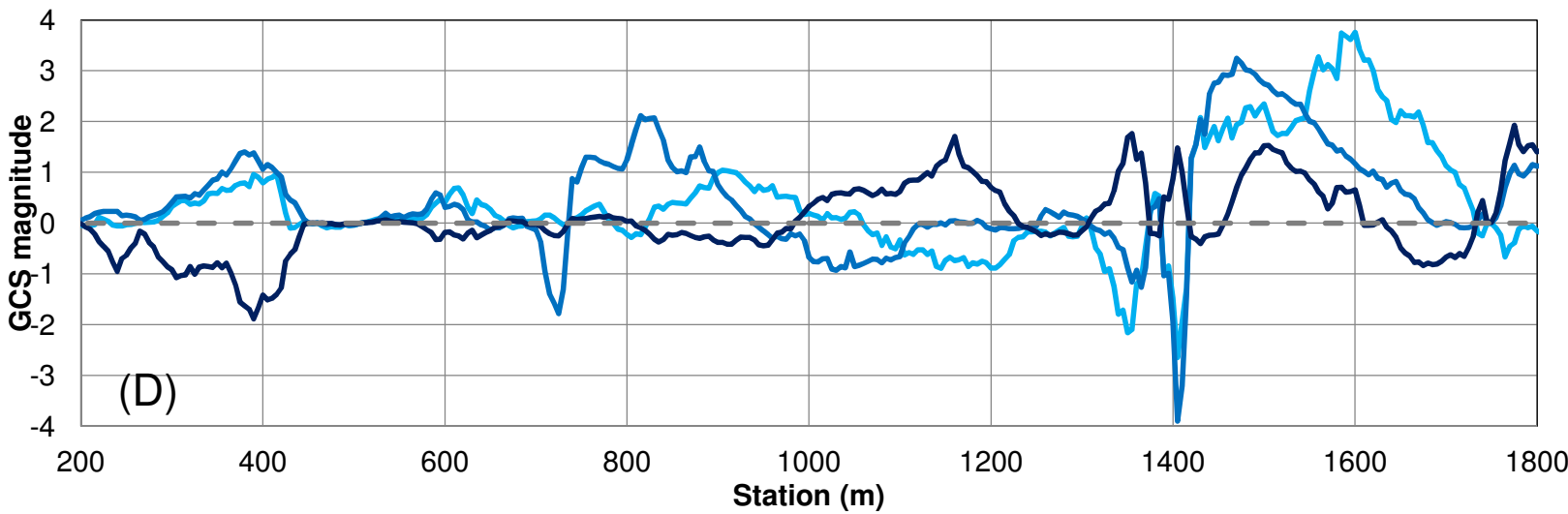
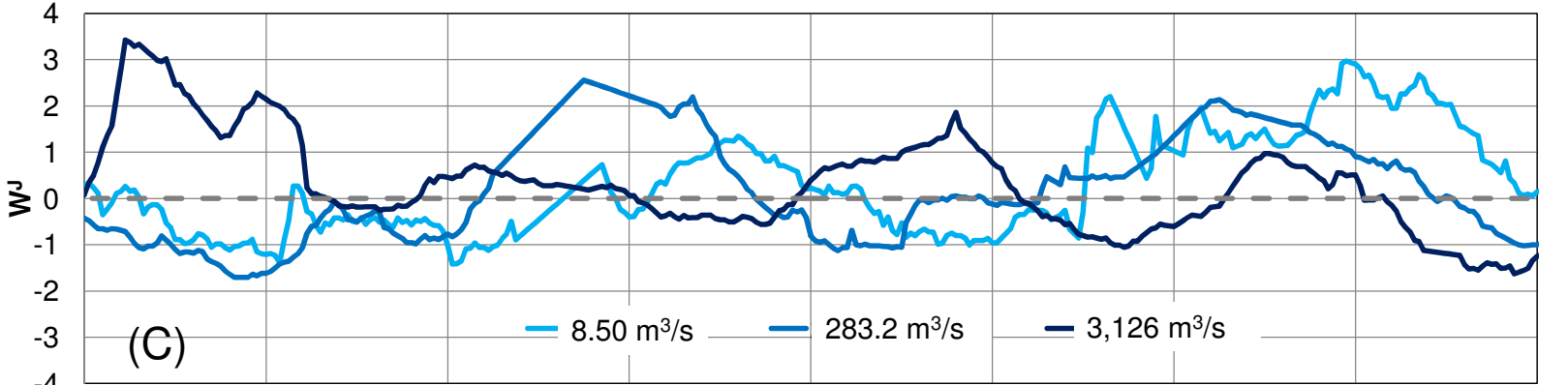
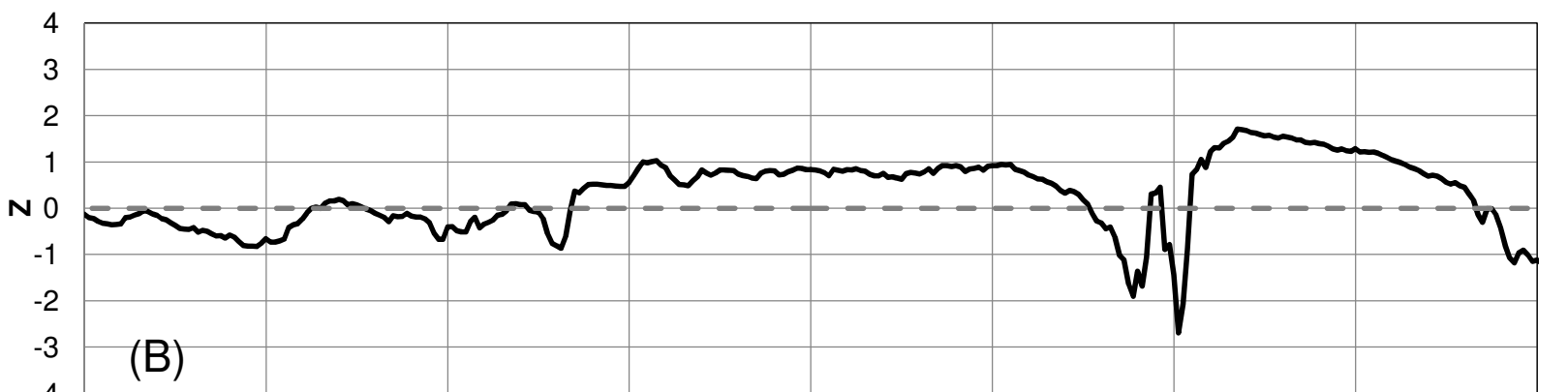
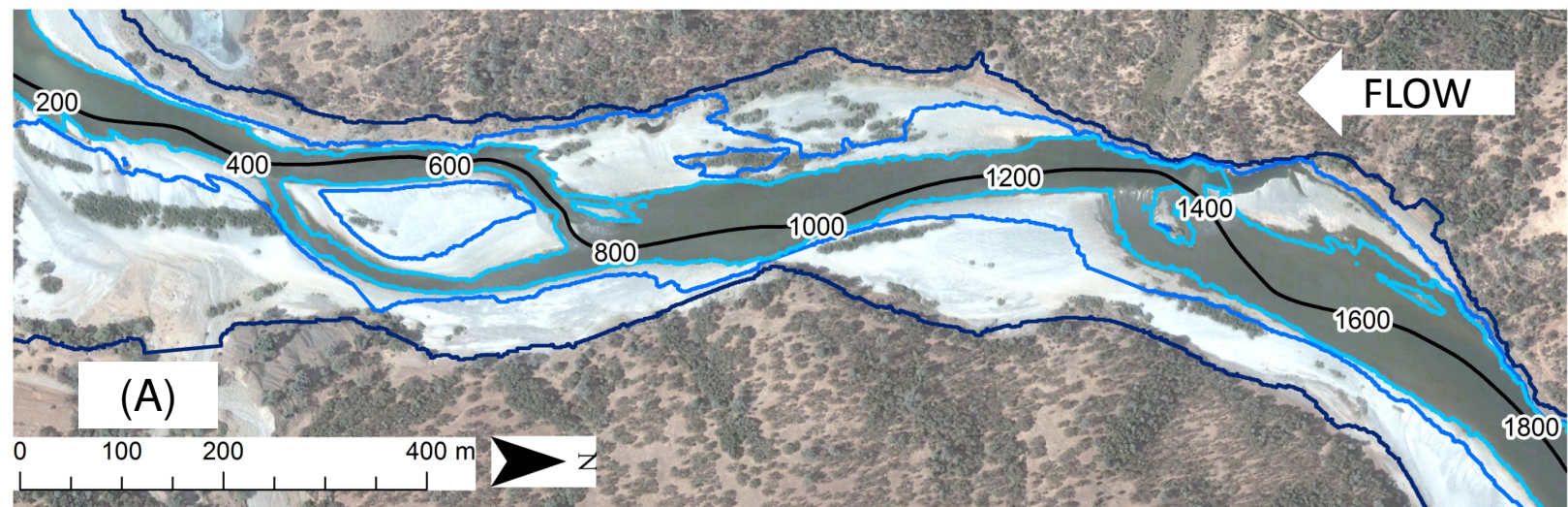
 $+W^j$ $-C(Z, W^j)$ $+C(Z, W^j)$ $-W^j$ $+C(Z, W^j)$ $-C(Z, W^j)$

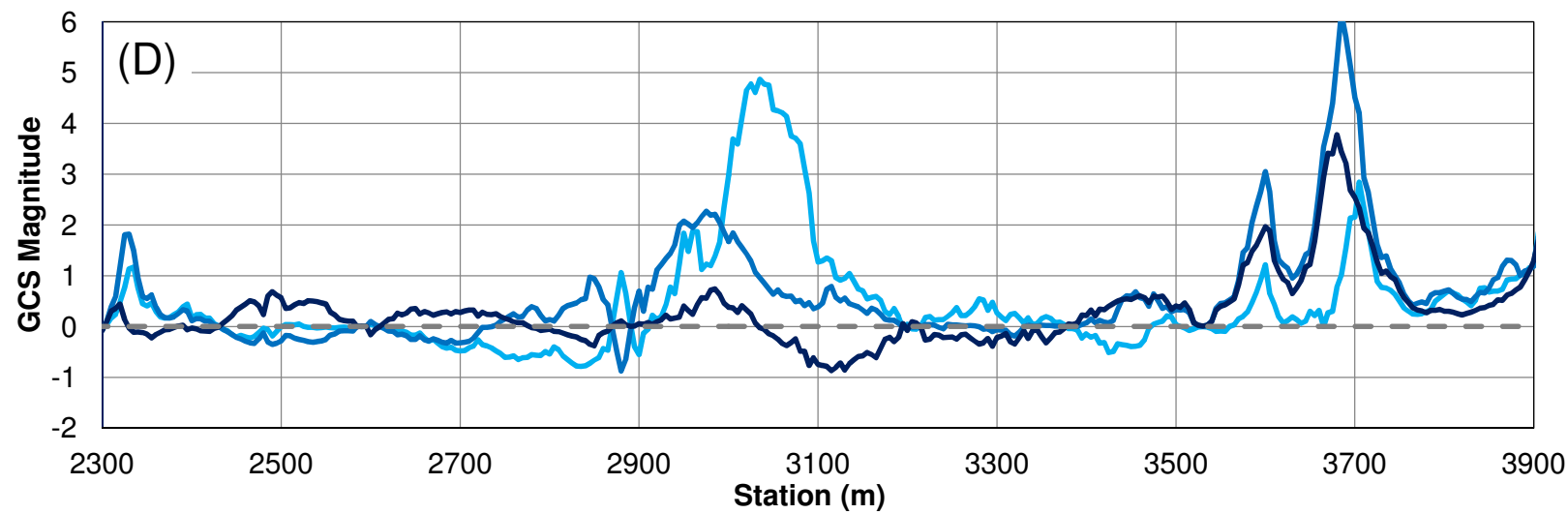
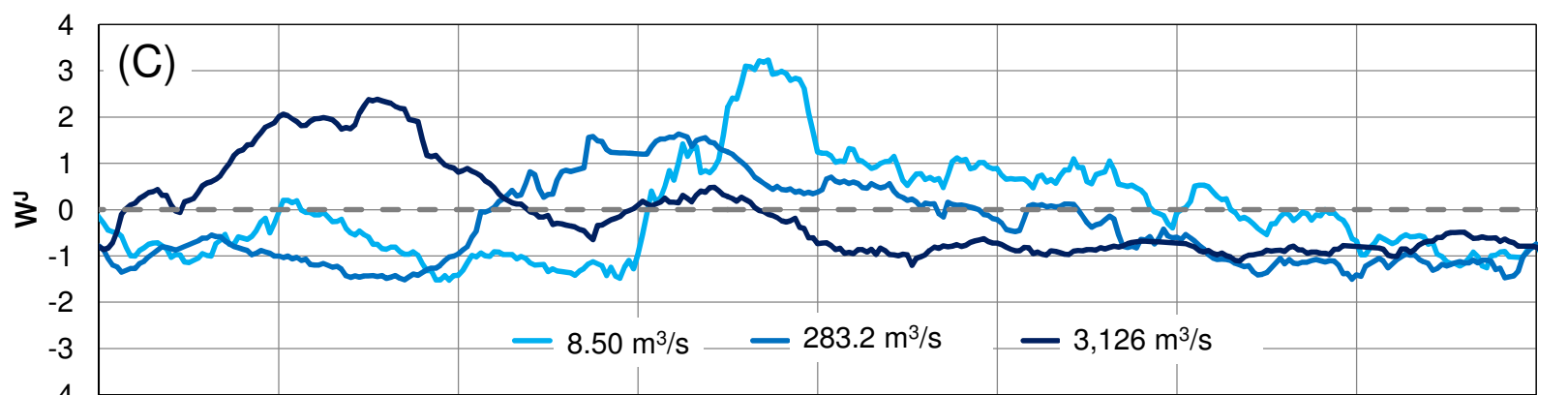
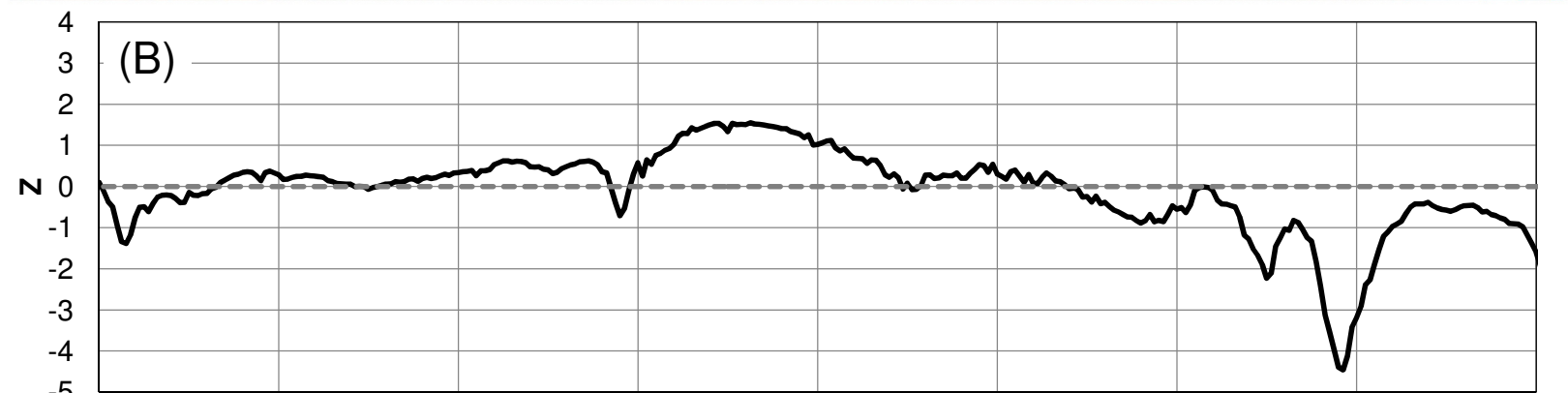
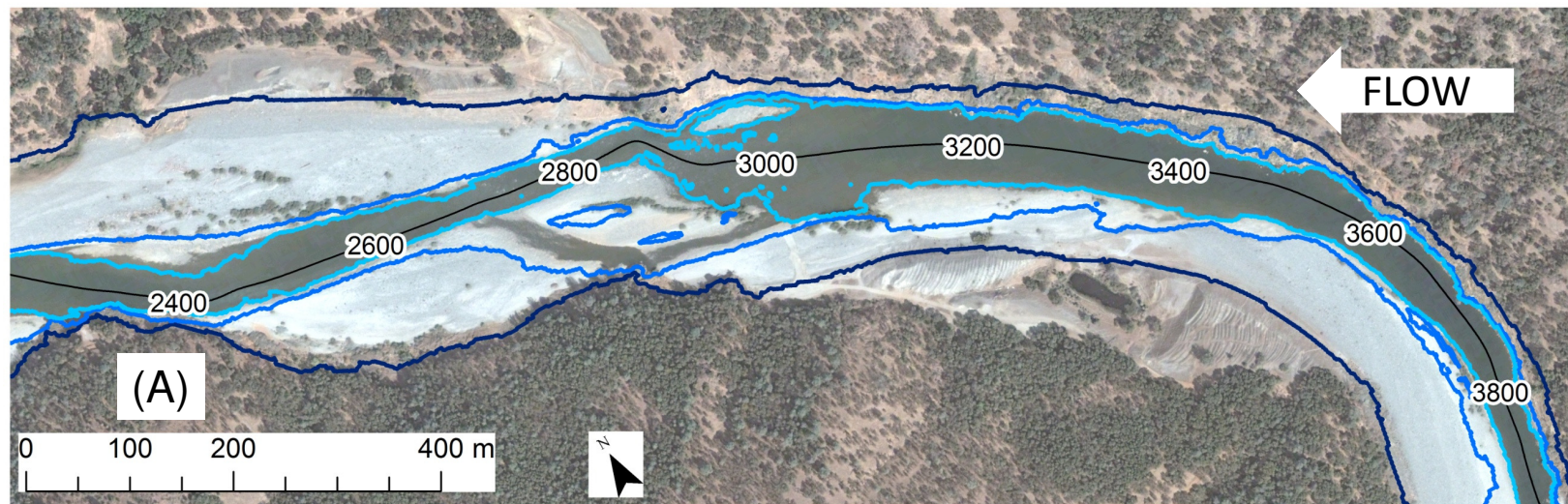
(B)

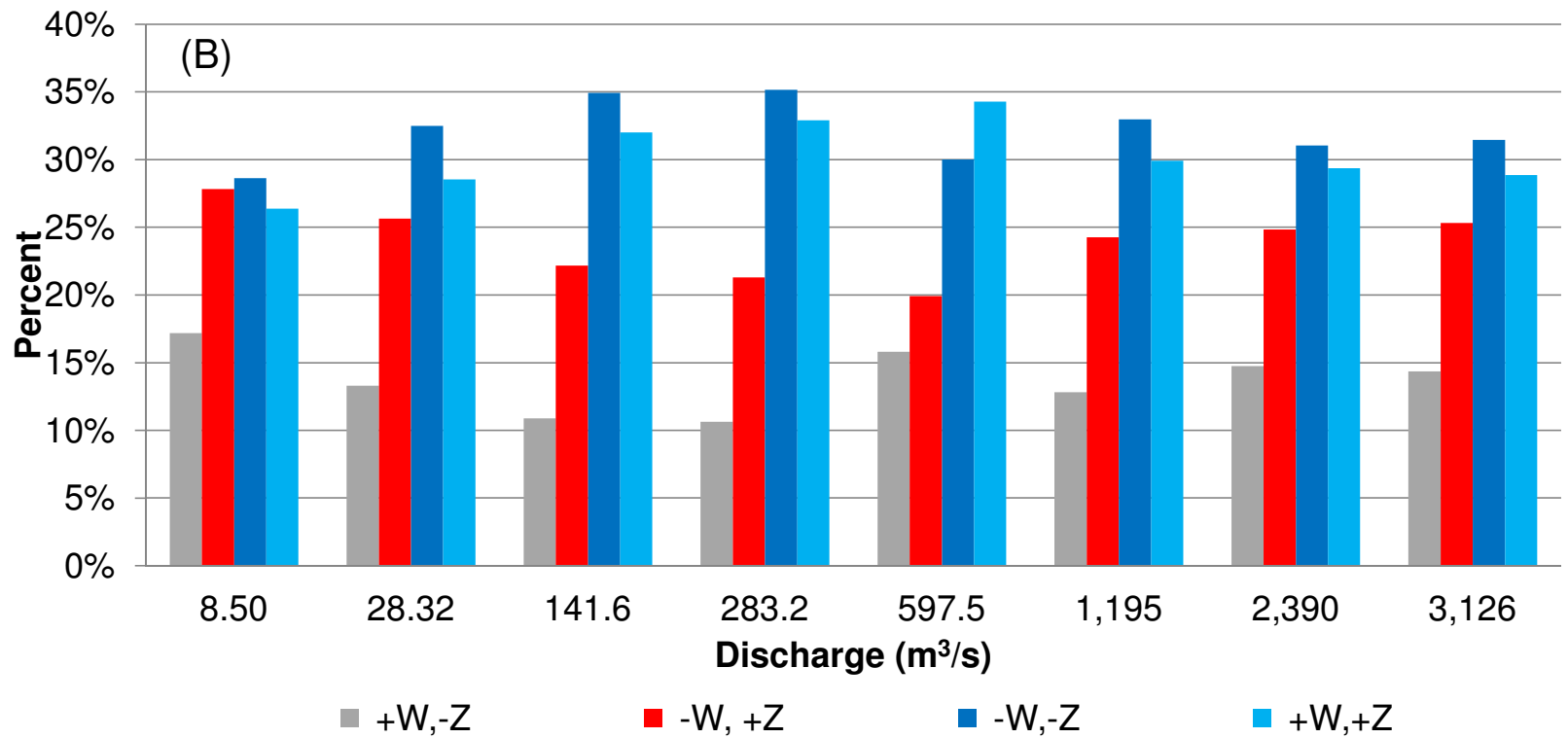
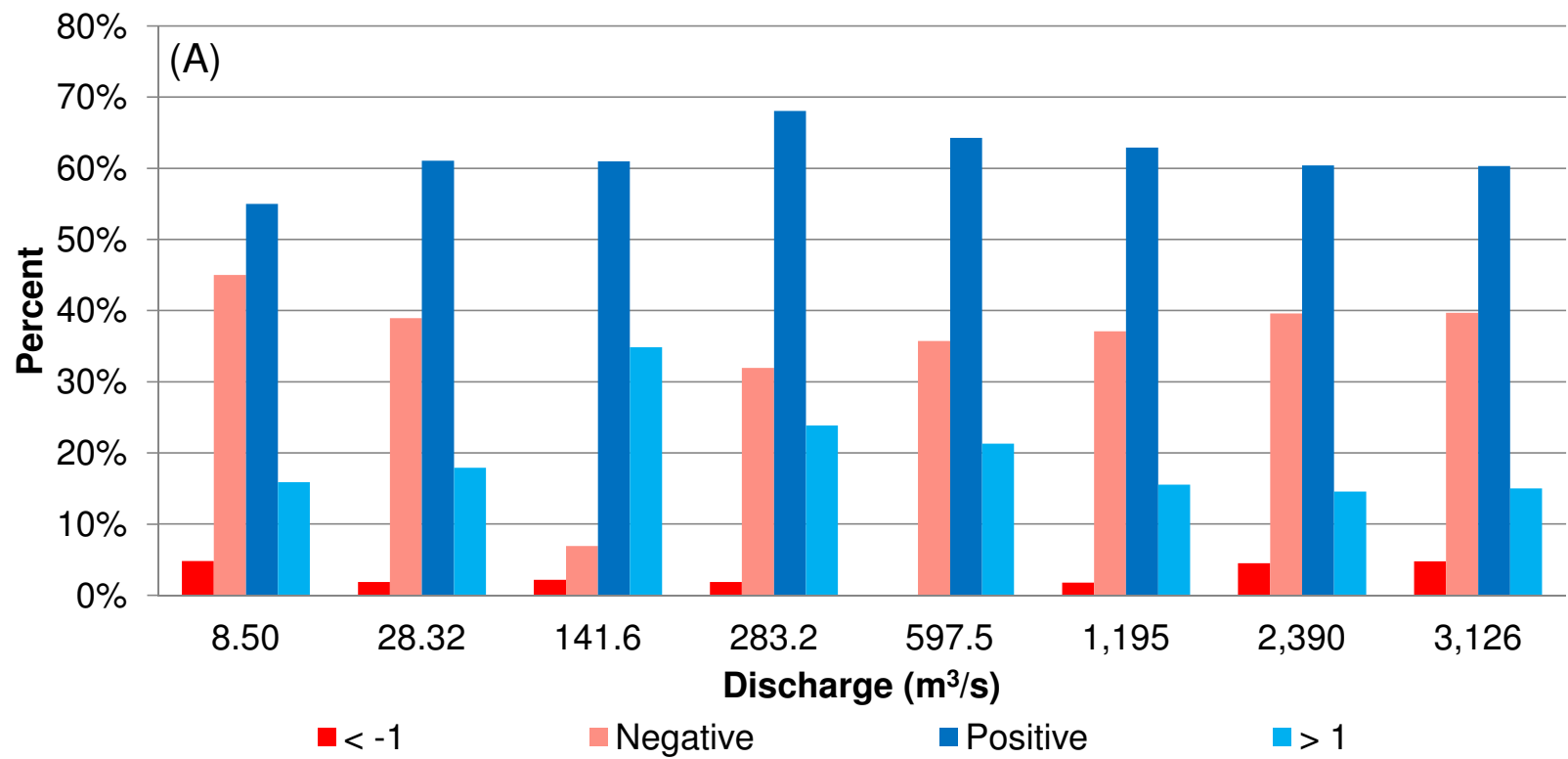


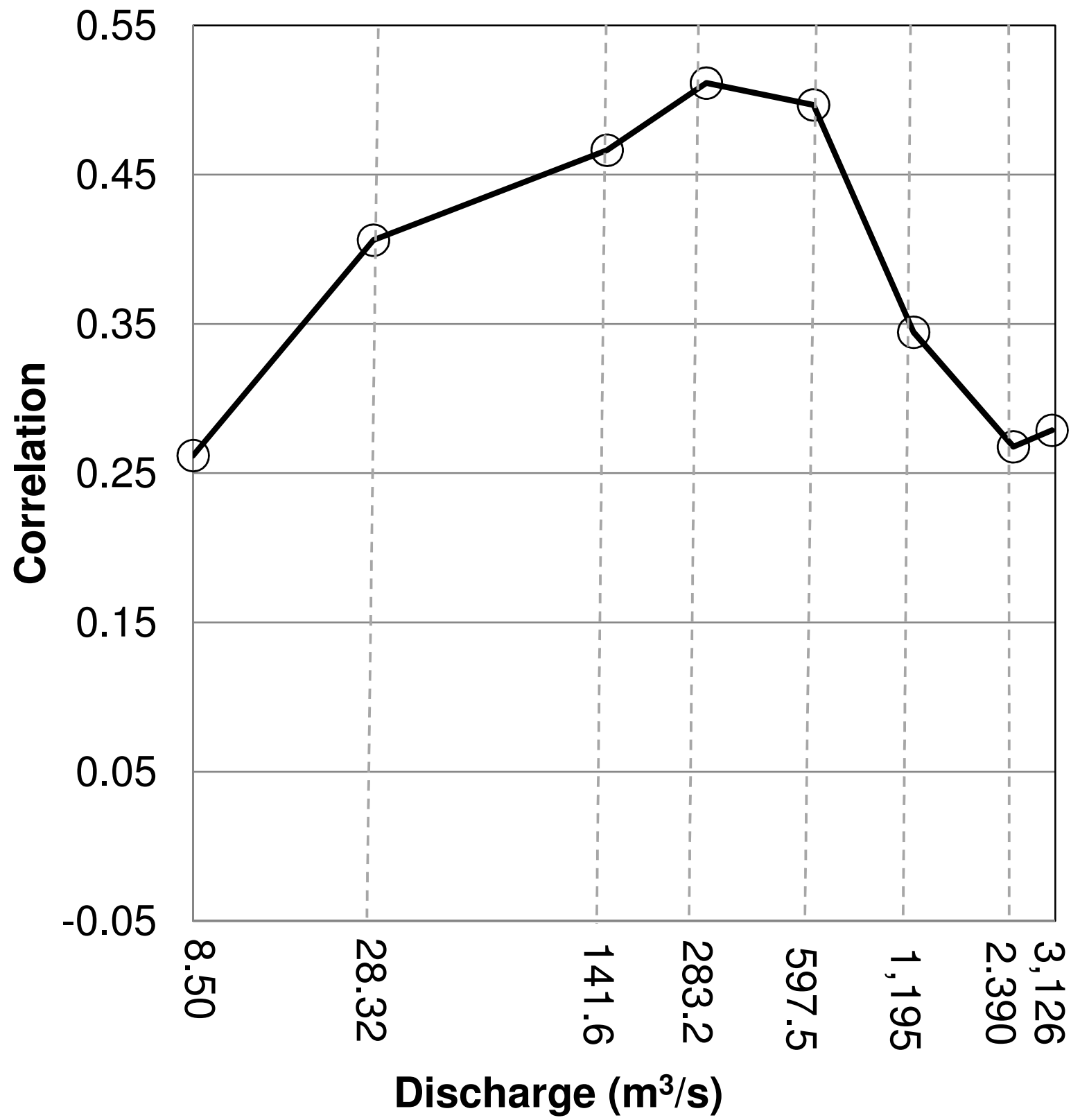
(C)

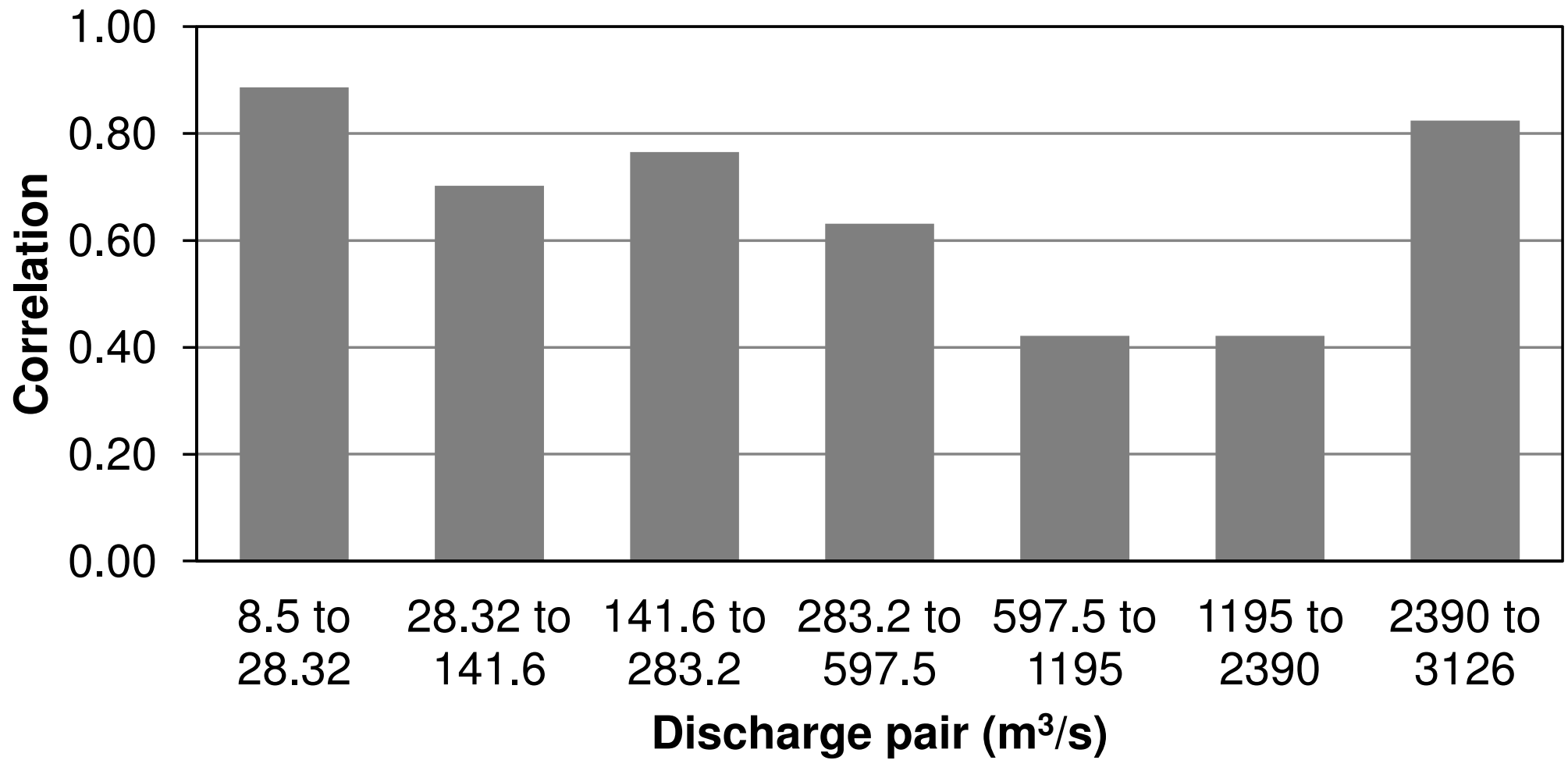












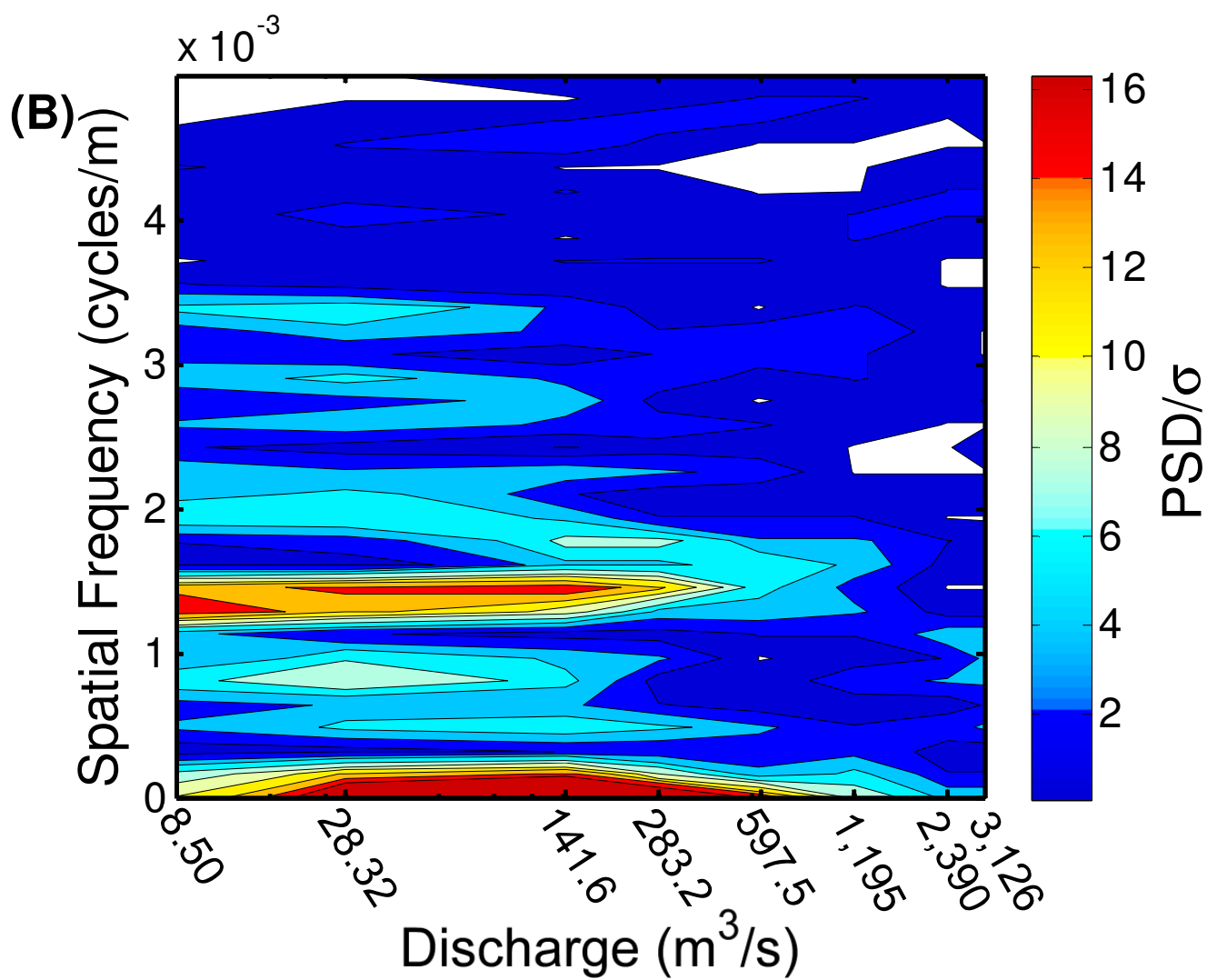
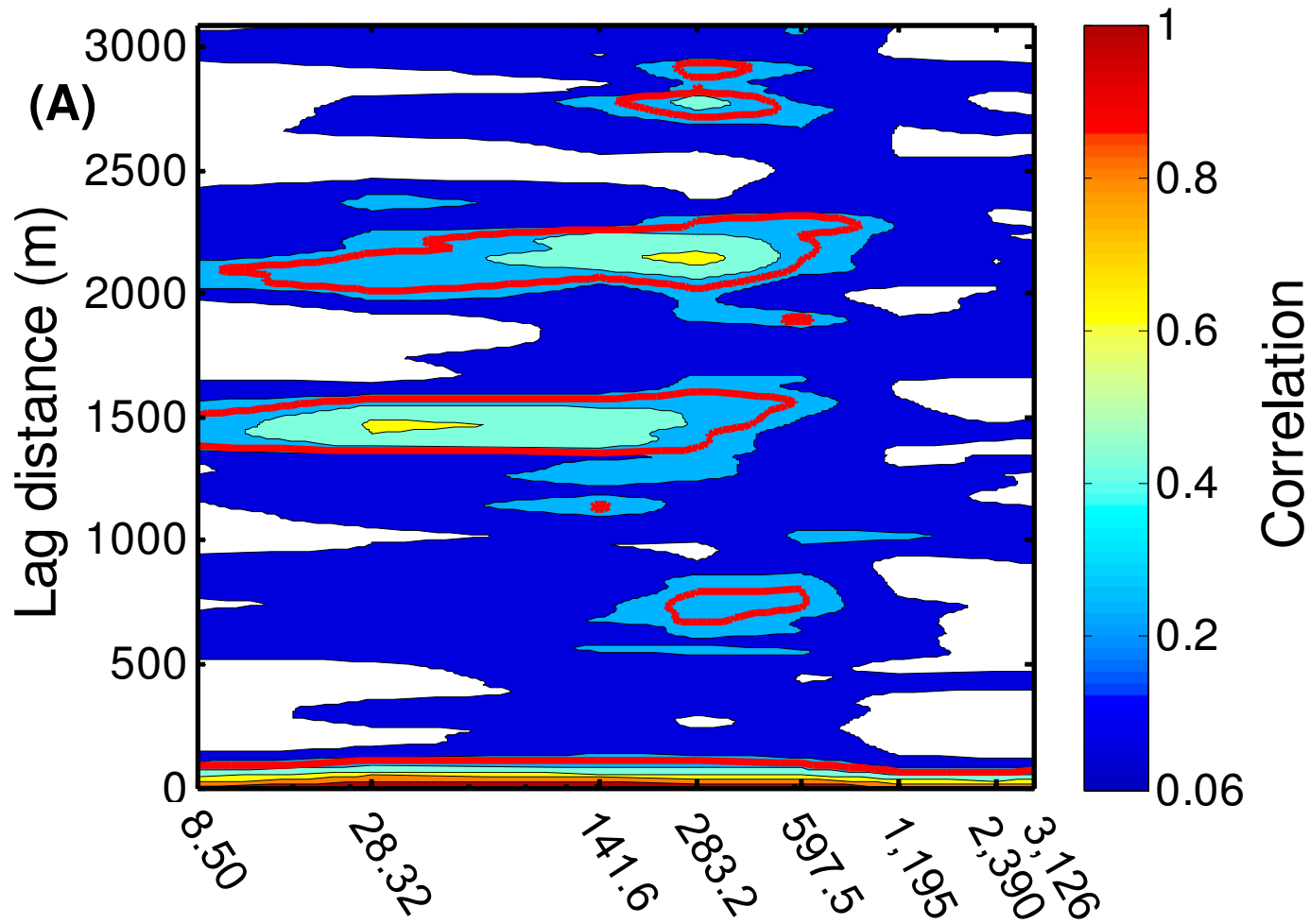


Table 1. Flows analyzed and their approximate annual recurrence intervals

Q (m³/s)	Approximate Recurrence Interval
8.50	1
28.32	1.03
141.6	1.2
283.2	1.5
597.5	2.5
1195	4.7
2390	12.7
3126	20

Table 2. Linear trend models and R² for Z and W^h used in detrending each series

Discharge (m ³ /s)	Top width		Bed elevation	
	Linear trend model	R ²	Linear trend model	R ²
8.50	$y = -0.0016x + 193.03$	0.0231	$y = 0.002x + 194.2$	0.8727
28.32	$y = -0.0025x + 234.27$	0.0429	$y = 0.002x + 194.26$	0.8713
141.6	$y = -0.003x + 301.61$	0.0423	$y = 0.0021x + 194.04$	0.8731
283.2	$y = -0.0002x + 332.87$	0.0002	$y = 0.0021x + 194.23$	0.8710
597.5	$y = -0.0101x + 528.6$	0.2286	$y = 0.0021x + 194.16$	0.8711
1,195	$y = -0.0133x + 665.02$	0.3037	$y = 0.0021x + 194.29$	0.8703
2,390	$y = -0.012x + 710.57$	0.2420	$y = 0.0022x + 193.92$	0.8736
3,126	$y = -0.0121x + 733.12$	0.2437	$y = 0.0022x + 193.94$	0.8733

